Exploring Zwitterionic Coronas as Alternatives to Traditional PEG Architectures for Improved siRNA Polyplex Pharmacokinetics and Tumor Delivery

By

Meredith A. Jackson

Thesis

Submitted to the Faculty of the

Graduate School of Vanderbilt University

in partial fulfillment of the requirements

for the degree of

Master of Science

in

Biomedical Engineering

December, 2016

Nashville, Tennessee

Approved:

Craig L. Duvall, Ph.D.

Todd D. Giorgio, Ph.D.

ACKNOWLEDGMENTS

I would like to thank my advisors, Dr. Craig Duvall and Dr. Todd Giorgio, for supporting me throughout this work. Thanks to Dr. Duvall for conceiving the original idea behind the project, for giving me scientific guidance throughout, and for encouraging me to persevere through the many interesting challenges it posed. I would also like to thank several key members of both the Duvall and Giorgio labs whose assistance was invaluable to this project. Thank you to Thomas Werfel for providing me with my initial training in the lab, for answering countless questions, and for weighing in on difficult problems. Thank you to my undergraduate colleagues, Ayisha Jackson, Zoe Johnson, and Elizabeth Curvino, for their assistance at various stages. Thank you to Kameron Kilchrist for assistance with intravital microscopy and to Samantha Sarett for assistance with flow cytometry. Thank you to Taylor Kavanaugh and Dr. Fang Yu for assistance with animal care and tail vein injections. Thank you to Mary Dockery and Stephanie Dudzinski for assistance with *in vivo* tumor uptake studies. Thank you to Dr. Mukesh Gupta and Dr. Eric Dailing for providing general chemistry-related guidance. Finally, I would like to extend a general thanks to all members of the Duvall, Giorgio, and Sung labs for creating such a supportive and positive environment in which to work.

I would also like to thank Dr. Don Stec for NMR training and assistance at various points in this project. Dynamic Light Scattering was performed using instrumentation in the Vanderbilt Institute of NanoScale Sciences and Engineering (VINSE), and Isothermal Titration Calorimetry measurements were performed using the Vanderbilt Center for Structural Biology core facilities. This work was supported by the Vanderbilt School of Engineering, the Department of Defense through DOD PRORP OR 130302, and by the National Science Foundation Graduate Research Fellowship under Grant No. 1445197.

TABLE OF CONTENTS

Page

LIST OF TABLES

LIST OF FIGURES

CHAPTER I

BACKGROUND

siRNA Therapeutics

The field of siRNA-based therapeutics has come a long way since the first discovery of these short, 19-30 base oligonucleotides with potent mRNA silencing abilities in *C. elegans* in 1998.[1] These siRNA molecules are active in the cytoplasm, where they bind to complementary mRNA at the RNA-induced Silencing Complex (RISC), and activate degradation of the mRNA transcript.[2] Because of their high specificity for target mRNA, siRNAs hold great potential for treatment of a variety of disease states while also minimizing off target side effects common with traditional, non-specific small molecule drugs. In the nearly 20 years since the discovery of siRNA, over 50 clinical trials with siRNA-based therapeutics have occurred [3]. The siRNAs used in these trials were designed to have IC 50 values in the nanomolar to picomolar range, making them extremely potent gene silencers[3].

While early clinical trials focused on local delivery of siRNAs for treatment of such ocular diseases as age-related macular degeneration, diabetic macular edema, and glaucoma, later trials have delivered siRNA systemically for treatment of liver-related diseases or cancers.[3, 4 5]

In each of these trials, siRNAs were encapsulated in nanoparticle-based systems. These carrier systems are often necessary because siRNAs are large, hydrophilic macromolecules with poor pharmacokinetics in their free form.[3] Upon intravenous injection, free siRNAs are rapidly degraded by nucleases in serum. Backbone modifications such as 2'-O-methyl modifications can prevent such fast nuclease degradation.[6] However, because of their size, siRNAs are also prone to glomerular filtration and therefore fast excretion via the kidneys.[7] Even if free siRNAs were to overcome these barriers, their negative charge results in extremely low tissue permeability,

making it difficult to impossible for free siRNA to pass through cell membranes and reach their targets. Additionally, any siRNAs taken up by cells would be trapped in endosomes and degraded in lysosomes, never reaching the RISC target in the cytoplasm.[2]

Nanoparticulate carriers pose a solution to the problem of poor systemic bioavailability of free siRNA. Nanoparticles can protect siRNAs from nuclease degradation, reduce glomerular filtration (due to their large size), and increase transport across cell membranes depending on their physicochemical properties.[3] In the field of nucleic acid delivery, traditional encapsulation methods can be divided into two main categories—viral delivery and non-viral delivery. [8] In the arena of non-viral particulate systems, the most common carrier systems are either lipid-based or polymer-based.[9] Typically, in these systems, the negative charge of siRNA is leveraged via complexation with a cationic lipid or cationic polymer, resulting in effective encapsulation within a carrier. Both polymer and lipid-based siRNA vectors have been studied in clinical trials and shown to effectively deliver siRNA to therapeutic site of action with promising mRNA knockdown results.[3] While both types of systems have their respective advantages and disadvantages, polymer-based systems may be less immunogenic than lipid-based systems, as the CALAA-01 clinical trial involving cyclodextrin-based delivery systems, had lower immunogenicity as compared to other clinical trials involving lipid-based systems.[10] Most lipid-based systems have been developed to target the liver preferentially to treat hepatic diseases, but such targeting is not necessarily optimal for treatment of cancer, where delivery to solid tumors is preferred.[11-14]

Nanocarrier Delivery for Cancer Therapeutics

Because of the strong role genetic mutations play in the development and progression of cancer, siRNA holds great potential for cancer therapeutics. It is believed that siRNA gene

silencing depends on the rate of cell division, however, posing a challenge in the arena of cancer therapies.[10, 15] For liver disease, because hepatocytes are relatively quiescent, silencing is more durable and only monthly treatment administration is necessary[15]. Cancer, on the other hand, is characterized by rapid division of cells, resulting in potential dilution of siRNA silencing effects.[15] Thus, the need for repeat administration of therapeutic siRNAs necessitates invention of optimal nanocarriers that are safe and reliable delivery vehicles.

Nanoparticle-based drug delivery vehicles are frequently used to target solid tumors passively via a phenomenon known as the enhanced permeation and retention effect (EPR). This phenomenon, first described by Maeda and colleagues in 1986, states that because of the fast rate of cancer growth and progression, blood vessels surrounding tumor tissue are often ill-formed, tortuous, and as a result, more permeable than normal vasculature, with larger pore sizes.[16] Nanoparticles with sizes around 50-200 nm can easily fit through vascular pores in tumor tissue, but not through vascular pores in normal tissue, making them selective for tumor tissue. [17, 18]This provides a great advantage for nanotechnology, because it theoretically reduces the likelihood of experiencing negative side effects based on cell death in normal tissues. In recent years, the EPR effect has been called in to question. Several researchers have argued that in humans, the EPR effect is extremely variable and unreliable, making it difficult to judge which patients might benefit from nanoparticle-based drug therapies.[19] However, results from early phase siRNA carrier clinical trials have indicated target mRNA knockdown and siRNA delivery to tumor tissues, providing great hope for the future of nanoparticle-based therapeutics in cancer as the nuances of the EPR effect continue to be explored and leveraged appropriately.[3, 10]

CHAPTER II

INTRODUCTION

Since their discovery in 1998, small interfering RNAs (siRNAs) have shown great promise as human therapeutics for a variety of diseases, including cancer, with many clinical trials completed or currently in progress.[1, 3, 10] However, because of the poor pharmacokinetic properties of free siRNA, there remains a major need for optimized nanoparticle carriers to improve their systemic bioavailability and delivery to solid tumors.[6, 9] Many cationic polymer systems have been developed to fill this need, but delivery challenges remain. Because of the relatively small fraction of cardiac output a tumor receives in the context of the entire body, a nanocarrier must remain in systemic circulation for extended periods in order to passively accumulate at the site of a tumor via the enhanced permeation and retention effect (EPR) enough to have a significant therapeutic effect at the target site.[20, 21]

Upon intravenous administration, an siRNA- polymer complex (polyplex), encounters a complex *in vivo* environment that can result in carrier destabilization or clearance by phagocytic cells as primary elimination mechanisms. [20, 22, 23] Polyplexes can disassemble in circulation when they encounter anionic heparin sulfates at the kidney glomerular basement membrane, or any number of serum proteins that might penetrate polymer layers and compete with electrostatic interactions between polymer and siRNAs.[23-25] Similarly, protein adsorption can also make nanocarriers more recognizable to macrophages of the mononuclear phagocyte system (MPS), resulting in phagocytosis or potential activation of the complement system if complement proteins adsorb.[22, 26-28] Nanocarrier surfaces, as the primary point of exposure to the *in* vivo environment, play a key role in how protein coronas form and therefore how particle biodistribution occurs.[29] As a result of these properties, as well as size and charge, it is a well-

known fact that most nanoparticulate systems ultimately end up in the liver and spleen, organs of the reticuloendothelial system (RES).

The most common and exhaustively explored method for increasing particle stability, reducing protein adsorption, and improving pharmacokinetics is the use of PEGylation. The importance of PEG molecular weight, architecture, and surface density for increasing particle circulation time has been widely studied.[30-39] However, equally well-documented is the fact that proteins can still penetrate PEG layers, resulting in opsonization, destabilization, rapid phagocytosis, and RES accumulation in spite of the added steric stabilization.[25, 30, 40, 41] Additionally, many studies have shown that PEG can be immunogenic and decrease overall cell uptake, including tumor cells.[40, 42] IgG and IgM have been shown to bind to PEG, enhancing complement activation.[40] PEG is also prone to the Accelerate Blood Clearance phenomenon (ABC), in which repeat injections of PEGylated carriers result in faster RES clearance due to immunogenic effects. [43-45]

An exciting alternative to PEGylation that is under-studied in the field of siRNA delivery is zwitteration of polyplex coronas. Zwitterionic surfaces are extremely hydrophilic and interact electrostatically with water as compared to PEG, which hydrogen bonds with water.[46-48] One type of zwitterion, in particular, phosphorylcholine, has found widespread use for anti-fouling applications and is an FDA-approved component of contact lenses and drug-eluting stents.[46, 49-51] Phosphorylcholine-based polymers are hemocompatible, easy to synthesize, and can mimic non-thrombogenic surfaces of red blood cells, which contain many phosphorylcholine groups. The use of zwitterions in various nanocarriers has improved *in vitro* stability, cell uptake, and in some, cases, *in vivo* pharmacokinetics.[52-57] While MPC has been incorporated into a few siRNA

or pDNA delivery vehicles for both *in vitro* and *in vivo* applications, it has never been directly compared to PEG architectures for *in vivo* pharmacokinetics or siRNA delivery to tumors.[56, 58-61]

Our previous work has focused on optimization of the core-forming block of polymers containing a balanced ratio of cationic and hydrophobic monomers (Dimethylamino ethyl methacrylate (DMAEMA) and Butyl Methacrylate (BMA)), respectively), for improved blood stability, bioactivity, and pH-responsive, endosomolytic properties of siRNA carriers.[62] These previously-optimized carriers have utilized a 5kDa linear PEG as their corona-forming block to improve polyplex stability.

In the present study, we have preserved the optimal core-forming components of our siRNA polyplexes but synthesized novel corona blocks in order to compare PEG to zwitterionic methacryloyloxy ethyl phosphorylcholine (MPC)-based polymers in terms of *in vivo* pharmacokinetics, as well as *in vivo* tumor accumulation and gene knockdown. In other work, we and others have sought to improve PEGylated nanocarrier pharmacokinetics through the use of a brush PEGylation architecture or high molecular weight Y-shaped PEGs, to varying degrees of success.[33, 34, 63, 64] Therefore, we also compare MPC coronas to these alternative PEG architectures in addition to our traditional linear polymer architecture.

To our knowledge, this is the first study to compare MPC-based siRNA polyplexes to traditional PEGylated siRNA polyplexes in terms of *in vivo* pharmacokinetics and anti-tumor activity. Additionally, we are the first to use intravital confocal microscopy to thoroughly characterize the impact of surface chemistry on *in vivo* pharmacokinetics of nanocarriers.

CHAPTER III

RESULTS AND DISCUSSION

Synthesis of Diblock Copolymers with Varied Corona Chemistries

In total, six diblock copolymers were synthesized with a pH-responsive core block composed of a random copolymer with an equimolar ratio of dimethylaminoethyl methacrylate (DMAEMA) and butyl methacrylate (BMA). The corona blocks consisted of a 5kDa linear PEG, a 20kDa linear Y-shaped PEG, a 10kDa zwitterionic MPC-based corona, a 20kDa zwitterionic MPC-based corona, a 10kDa poly(ethylene glycol) methyl ether methacrylate (POEGMA) block, or a 20kDa POEGMA (**Figure 1**).

The 5k linear PEG, 10k MPC, and 10k POEGMA corona lengths were chosen because they were the shortest corona lengths that would form micellar structures using these materials. The 20k MPC and 20k POEGMA were chosen as standards to compare to the 20kDa Y-shaped PEG, which has previously shown superior pharmacokinetics to shorter PEG coronas[33].

For the linear PEG-containing polymers, the core block was RAFT polymerized from a linear PEG5k or linear Y-shaped PEG 20k macroCTA. For the MPC or POEGMA-containing polymers, the core block was RAFT polymerized first, followed by a second, facile RAFT polymerization of a corona-forming block of appropriate length. Due to the advantages of RAFT polymerization, all polymers had low polydispersity and were easily synthesized at the desired block lengths (**Table 1**).

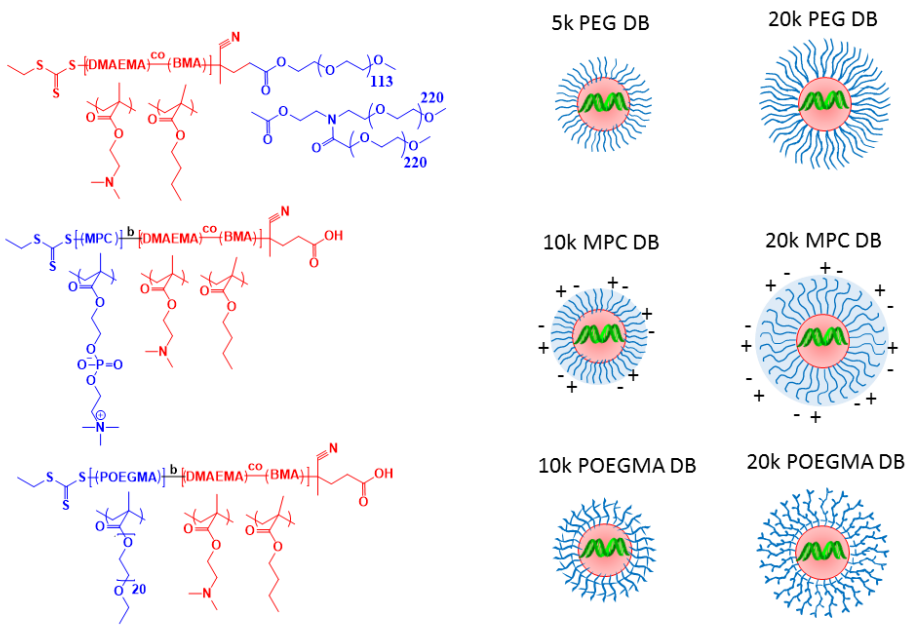

Figure 1. Six polyplexes with different surface chemistries. *All polyplexes contain the same core block consisting of DMAEMA and BMA, with different corona blocks as pictured. Polymer structures are displayed on the left, with core block in red and corona block in blue.*

Polymer	Total MW (g/mol)	Corona MW (g/mol)	% BMA	% DMAEMA	PDI
5k PEG DB	28636	5000	50	50	1.021
20k PEG DB	43353	20000	50	50	1.071
10k MPC DB	34129	10177	51	49	*
20k MPC DB	45044	21092	50	50	*
10k POEGMA DB	34171	11716	47	53	1.156
20k POEGMA DB	42619	18667	49	51	1.296

Table 1: Polymer Synthesis Results*. All polyplexes were synthesized at the desired corona block lengths with 50:50 molar ratios of DMAEMA:BMA. Polydispersity indices were low. * MPC polymers were not analyzed with GPC due to insolubility in mobile DMF phase.*

Synthesis and Stability Characterization of siRNA Polyplexes

To form polyplex micelles, polymer and siRNA were mixed at various N:P ratios at low pH, allowed to complex 30 min, and then the pH was raised to 7.4 to allow for spontaneous micellization. The results of a Ribogreen assay evaluating the encapsulation efficiency of these polyplexes shows that for all of the polyplexes except 20k POEGMA DB, siRNA was almost completely encapsulated at an N:P ratio of 5, but the highest encapsulation efficiencies (~80%) were achieved at N:P of 20 (Figure 2A). Additionally, we found that all of the polyplexes had higher stability at N:P 20 than N:P 10 after a 5 min incubation with heparin sulfate salts (Figure 2B). Thus, the remaining studies were carried out using an N:P ratio of 20.

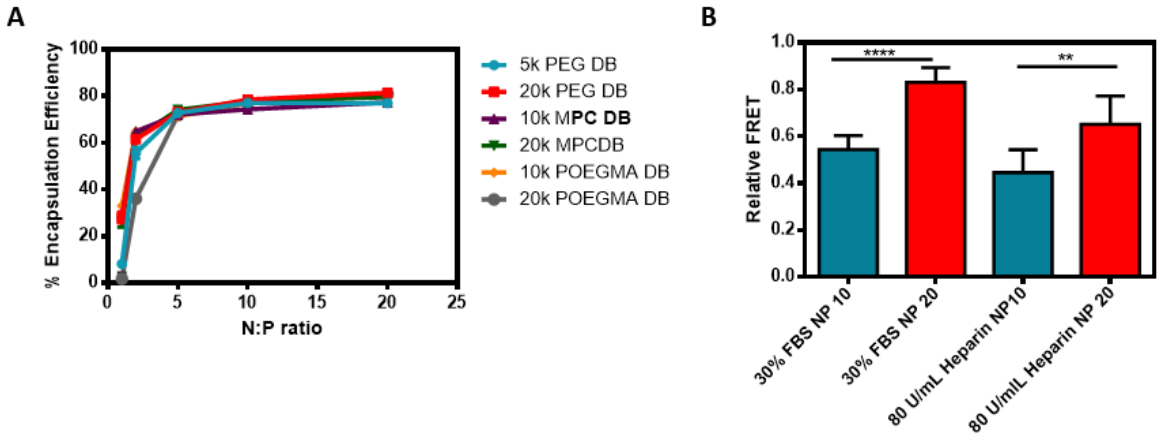

Figure 2: Polyplex siRNA encapsulation efficiency and overall stability *is highest at N:P 20. A) Ribogreen assay reveals ~80% encapsulation efficiency at N:P 20. B) Average stability of all polyplexes at N:P 10 vs N:P 20 in 30% FBS or 80 U/mL Heparin. P<0.01.*

Importantly, despite their varied corona molecular weights and characteristics, all polyplexes had sizes close to 100 nm and near-neutral zeta potentials. Thus, although size and

surface charge are known to highly affect pharmacokinetics[28], these factors did not vary significantly between each polyplex (Table 2).

Polyplex	Avg Size (d.nm)	Avg Zeta Potential (mV)	PDI
5k PEG DB	133.4	0.153	0.248
20k PEG DB	102.4	0.868	0.265
10k MPC DB	154.4	-2.94	0.230
20k MPC DB	114	-0.914	0.220
10k POEGMA DB	109.3	0.699	0.210
20k POEGMA DB	116.6	-2.86	0.535

Table 2: Polyplex Size, Zeta Potential, and Polydispersity. *All polyplexes were of uniform size and near neutral zeta potentials.*

Polyplex size and stability were further evaluated by introducing various salt concentrations into polyplex buffer. Figure 3 shows that the 20k MPC DB and 20k PEG DB polyplexes appeared most resistant to increasing salt concentrations based on dynamic light scattering traces, while the 5k PEG DB and POEGMA corona polyplexes were much less stable, losing their uniform size distribution and de-complexing at 0.25 M NaCl. This result indicated that larger coronas seemed to improve stability, but in the case of POEGMA-based polyplexes, increasing corona size did not improve stability.

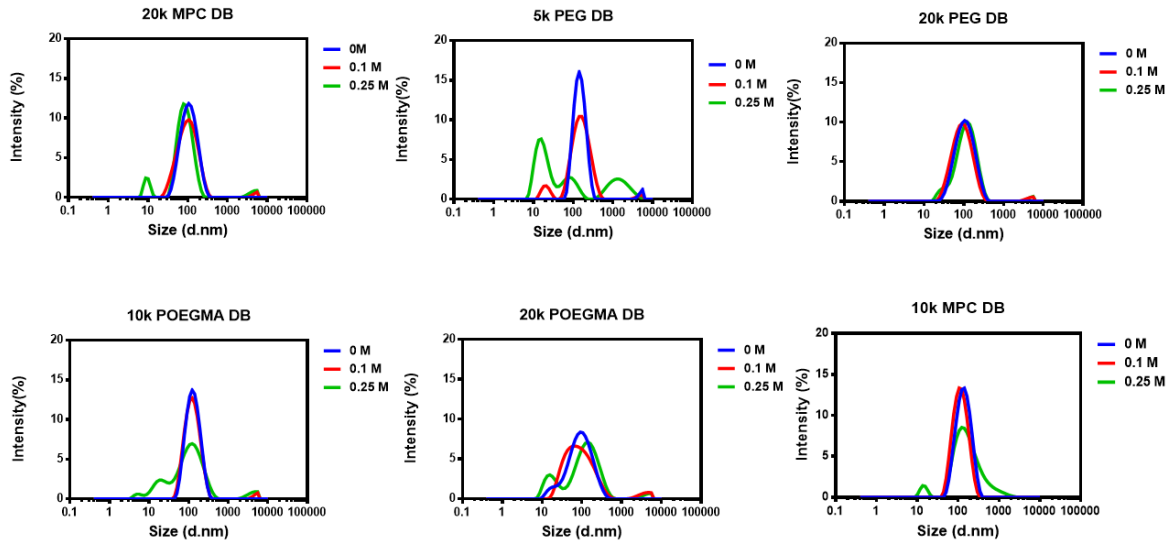

Figure 3: Polyplex Stability in Increasing Salt Concentrations. *Dynamic Light Scattering of polyplexes after introduction of 0, 0.1, or 0.25 M NaCl reveals superior stability properties of 20k MPC DB and 20k PEG DB.*

In order to maximize polyplex accumulation at the site of the tumor, it is vital to design polyplexes that resist destabilization for as long as possible in the bloodstream.[21] Two of the main sources of polyplex instability in intravenous circulation include serum proteins and anionic heparan sulfates in the kidney glomerular basement membrane.[22-24] We hypothesized that our novel polyplex corona chemistries might improve polyplex stability in response to these challenges. We therefore co-encapsulated DNA containing Alexa Fluor -488 or Alexa Fluor-546 fluorophores in the polyplex core and measured their FRET (forster resonance energy transfer) signal while simultaneously incubating polyplexes with varied amounts of either FBS or heparin sulfate (**Figure 4A and 4B**). Higher FRET signal indicated polyplex stability while decreased FRET signal indicated that the polyplexes had partially fallen apart in solution. In 10% serum, all polyplexes remained equally stable over time. However, at higher FBS concentrations, it

becomes clear that the novel polyplex coronas are better than linear 5k PEG at resisting destabilization. In the presence of heparin sulfate, the 20k Y-shaped PEG was clearly the most stable polyplex, but it was closely followed by the zwitterated polyplexes and the shorter POEGMA corona polyplex. Both the short 5k PEG and the 20k POEGMA polyplexes were least resistant to the heparin sulfate challenge. Thus, the most of the novel coronas provided the siRNA polyplexes with enhanced stability over the 5k PEG corona polyplexes. In the case of the 20k POEGMA DB, which appears less stable than the other high molecular weight coronas, it is likely that the bulky side chains may be too large for enhanced polyplex stability.

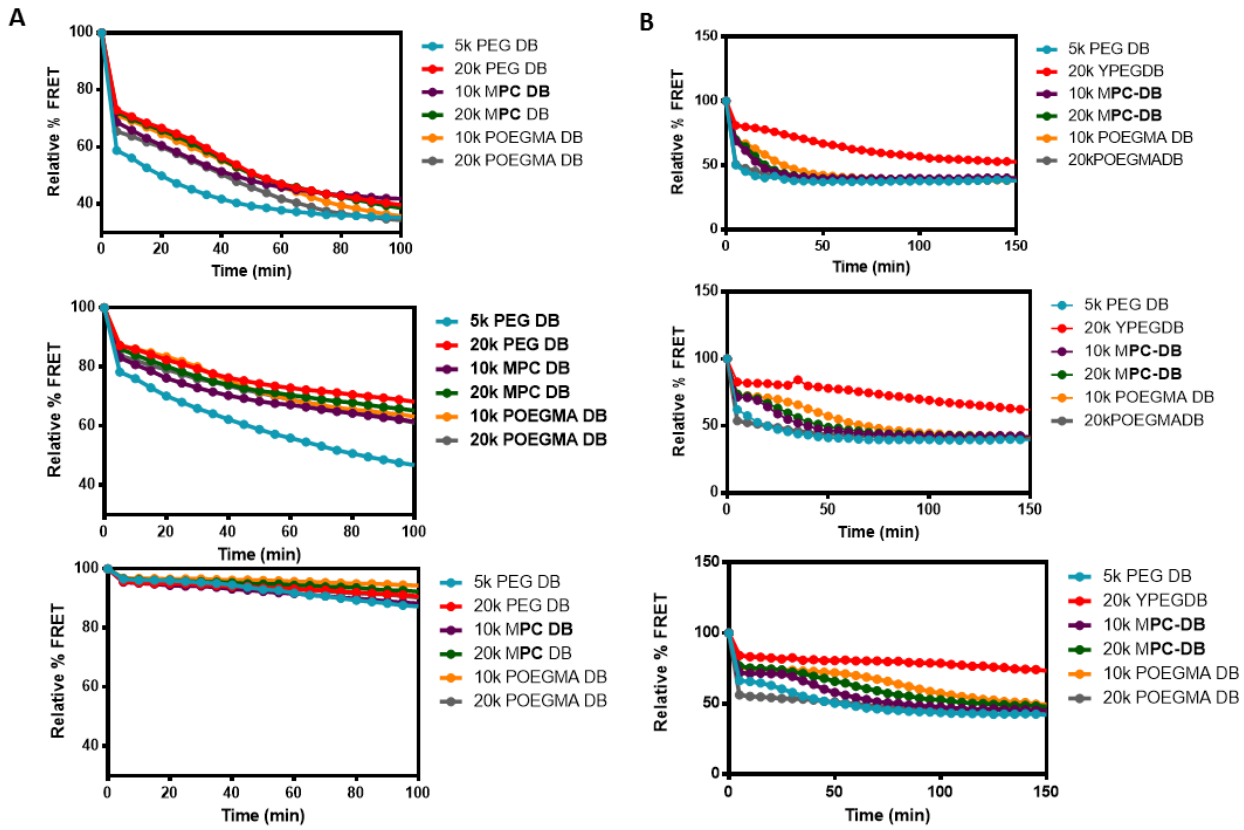

Figure 4: Polyplex Stability over Time. *A) Polyplexes incubated in 50% (top), 30% (middle), or 10% (bottom) FBS over 100 minutes show that most novel coronas improved FBS stability over 5k PEG DB. B) In 80 U/mL, 40 U/mL, and 10 U/mL heparin salts, 20k PEG DB maintained greatest stability levels.*

In vitro Characterization

Prior to our *in vivo* comparison of zwitterionic and PEGylated coronas, each polyplex was first evaluated for key *in vitro* properties to confirm their bioactivity and pH-responsiveness. Based on a red blood cell hemolysis assay described previously[65], each of the polyplexes showed endosomolytic activity at pH values at or below 6.8, corresponding to pH's found in the endolysosomal pathway, but no hemolytic properties at the physiological pH of 7.4 (**Figure 5A**). Because the pH-responsive behavior of these polyplexes is controlled by their core blocks, it is unsurprising that the different coronas did not differentially impact endosomolytic behavior.

All polyplexes were evaluated for cytotoxicity using luciferase expressing NIH 3T3 fibroblasts (**Figure 5B**). At 48 hours post-treatment, all cells maintained 87% or greater viability, indicating that none of the polyplex coronas increased cytotoxicity of these formulations.

We also evaluated knockdown of the model gene luciferase in MDA-MB 231 cells by delivering siRNA against luciferase in each type of polyplex (**Figure 5C**). At 48 hours post treatment, cells exposed to 5k PEG, 20k PEG, or either zwitterated corona all retained less than 10% luciferase activity (90% knockdown). For the POEGMA-based coronas, knockdown levels were less dramatic. 10k POEGMA achieved only around 50% knockdown, while 20k POEGMA-based polyplexes did not show any significant knockdown levels. This result suggests that the POEGMA-based coronas reduced *in vitro* bioactivity of polyplexes

Percent uptake of polyplexes by MDA-MB 231 breast cancer cells was also evaluated *in vitro* (**Figure 5D**). For the zwitterated coronas, 20k PEG, and 10k POEGMA coronas, 100% of cells were positive for polyplexes. For 5k PEG DB, this number was slightly lower (a significant decrease), and it was even lower for 20k POEGMA DB. Because this data correlates well with previous stability data, it suggests that the stability properties of the different coronas played a

more important role in cell uptake at 24 hours than the steric properties of the coronas themselves.

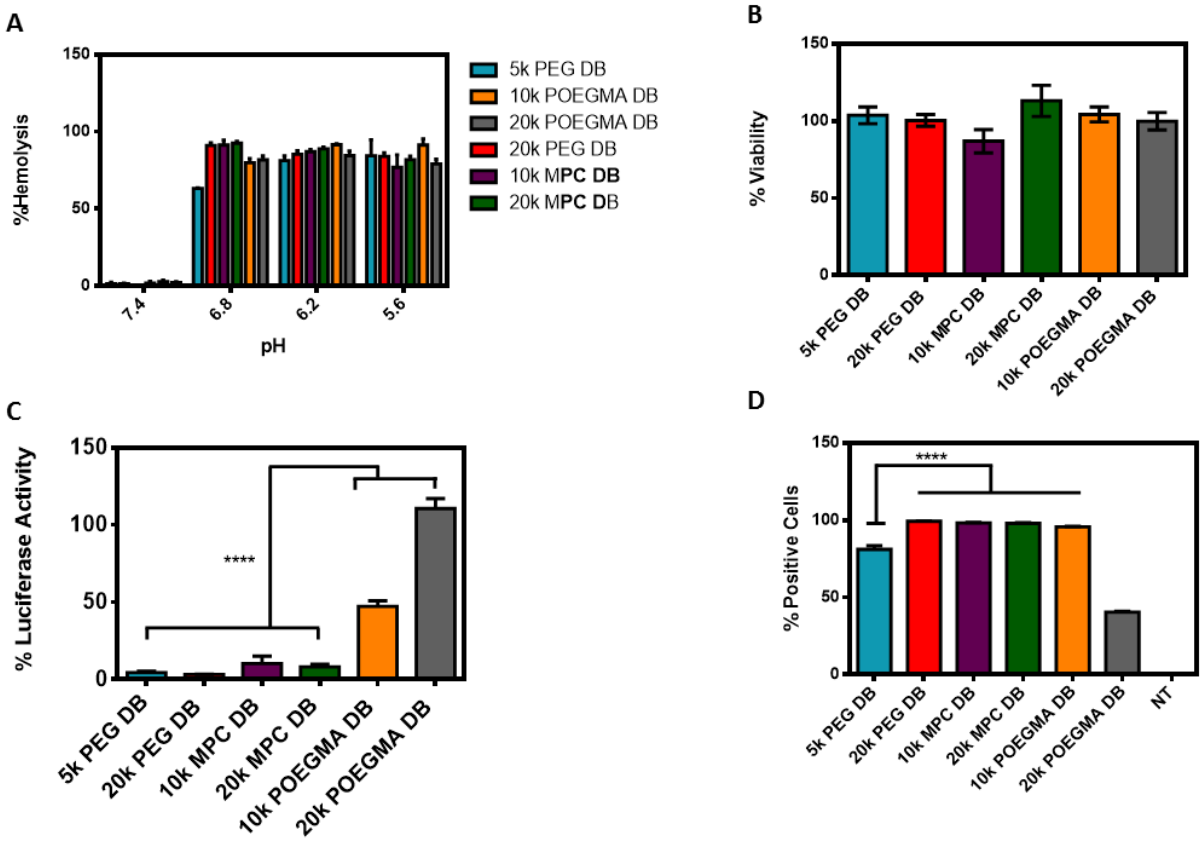

Figure 5: ***In vitro Polyplex Characterization.*** *A) All polyplexes retained similar pH-responsiveness at pH ranges tested in hemolysis assay B) Polyplexes did not damage cell viability of NIH 3T3 fibroblasts at 100 nM siRNA. C) Luciferase knockdown in MDA-MB231 cells was significantly improved for linear PEG and zwitterionic coronas, $p<0.01$. D) All novel polyplex coronas improved cell uptake over 5k PEG except 20k POEGMA, $p<0.01$.*

Protein Adsorption

Both PEGylation and zwitteration are designed to reduce protein adsorption to nanocarriers, because proteins mediate several nanocarrier clearance mechanisms. In general,

protein adsorption can make nanocarriers more identifiable to macrophages of the MPS or destabilize polyplexes, as discussed above. Similarly, if the proteins adsorbed are complement proteins like C3b, they can initiate a complement cascade further recruiting immune cells and promoting rapid clearance.[26] We used two methods to evaluate how PEGylation and zwitteration might differentially affect protein adsorption---isothermal titration calorimetry and a hemolysis-based complement assay.

Isothermal titration calorimetry (ITC) is an extremely sensitive method of assessing the thermodynamics of interaction between a protein and ligand.[66, 67] In ITC, a protein solution is slowly titrated into a solution of polyplexes, and changes in heat resulting from their interaction are recorded. These heat changes can be extrapolated to measure entropy, enthalpy, and Gibb's free energy of interaction between the protein and polyplexes. ITC has been used in the past to characterize protein adsorption to many different types of nanocarriers.[66, 67] It is especially valuable for polyplex evaluation because siRNA polyplexes do not sediment, and therefore they cannot be evaluated by most traditional protein adsorption assays. Albumin was here used as a model for serum proteins, since it makes up the largest component of human serum. Overall, each polyplex, whether PEGylated or zwitterated, had a positive Gibb's free energy of interaction with albumin (**Figure 6A**). This indicates that albumin binding was not spontaneous and therefore unfavored. However, the magnitude of (delta G) values were higher for the higher molecular weight coronas as compared to their lower molecular weight counterparts, indicating albumin adsorption was least favorable for these coronas. The 20k linear Y-shaped PEG corona had the largest dG values of any polyplex and was significantly higher than any other polyplex. It was followed by the 20k MPC polyplex, indicating that the 20k PEG corona was slightly more protein resistant than the 20k MPC corona. All polyplexes were compared to a positive control

polyplex containing cationic DMAEMA in its corona. This cationic control showed extremely negative dG values indicating a highly favorable interaction with albumin.

In order to evaluate potential complement activation by the various corona chemistries, we used a hemolytic assay modified from Bartlett and colleagues.[66] Polyplexes were incubated with various dilutions of human complement sera and then antibody-sensitized sheep erythrocytes were added to each mixture. If complement proteins do not adsorb to polyplex coronas, then they are free to lyse the erythrocytes. However, if complement adsorption does occur, red blood cell lysis is reduced as fewer proteins are available to cause lysis. For all polyplexes, we did not observe significant differences in lysis compared to the complement only protein controls, meaning that complement adsorption was negligible (**Figure 6B**). The cationic DMAEMA corona control polymer, on the other hand, showed extremely reduced lysis compared to the complement only control, indicating significant adsorption, as expected. The 20k POEGMA corona polyplex exhibited slightly increased lysis levels compared to the protein only control, probably as a result of its greater instability in serum. Thus, overall, the novel coronas do not display significant levels of complement activation.

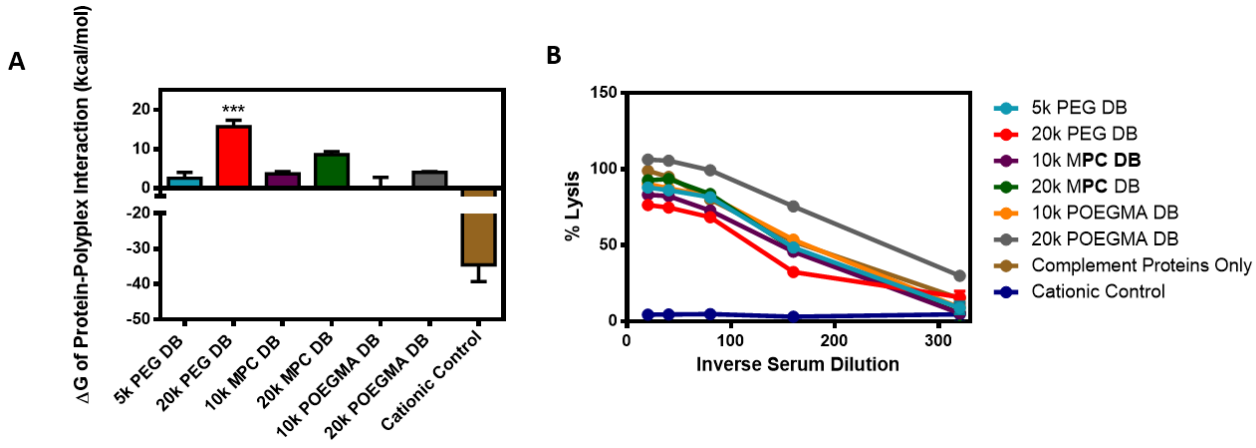

Figure 6*: Polyplex-Protein Interactions*. *A) Isothermal Titration Calorimetry of polyplexes indicated significantly less favorable BSA interaction for 20k PEG DB than for other polyplexes,*

p<0.01. B) Negligible complement protein adsorption was observed for all polyplex surface chemistries.

In Vivo Pharmacokinetics

While several *in* vitro methods can assist in predicting *in vivo* stability, the best way to identify potential differences between zwitterated and PEGylated polyplex coronas is through *in* vivo pharmacokinetic studies. Traditional methods of characterizing nanocarrier pharmacokinetics have relied on multiple blood draws and extrapolation to determine initial nanocarrier blood concentrations. Intravital confocal laser scanning microscopy, on the other hand provides real time second-by-second tracking of fluorescence in the mouse ear blood vessels, while using fewer animals.[68, 69] It provides a more thorough quantification of particle pharmacokinetics and is therefore a more accurate way to discern differences between PEGylated and zwitterionic coronas. For this study, polyplexes were loaded with Cy5-conjugated DNA and the fluorescence signal tracked for 20 minutes.

Intravital microscopy revealed superior pharmacokinetic properties for 20k PEG DB and 20k MPC DB polyplexes (**Figure 7A-D**). Qualitative differences from representative ear images can be visualized in **Figure 8.** Pharmacokinetic half-lives for each of these polyplexes were around 22 minutes (20k PEG DB) and 26 minutes (20k MPC DB), while half-lives for all other polyplexes ranged from 5-8 minutes (**Table 3**). Area under the curve for these polyplexes, when extrapolated to infinity, was very significantly highest for 20k MPC DB and 20k PEG DB, though there were no significant differences between these two coronas. Similarly, these two polyplexes also exhibited the slowest clearance values. Based on the intravenous

pharmacokinetic signal from these polyplexes, it appears that only the higher molecular weight zwitterionic and linear PEG coronas retained their stability for an extended period.

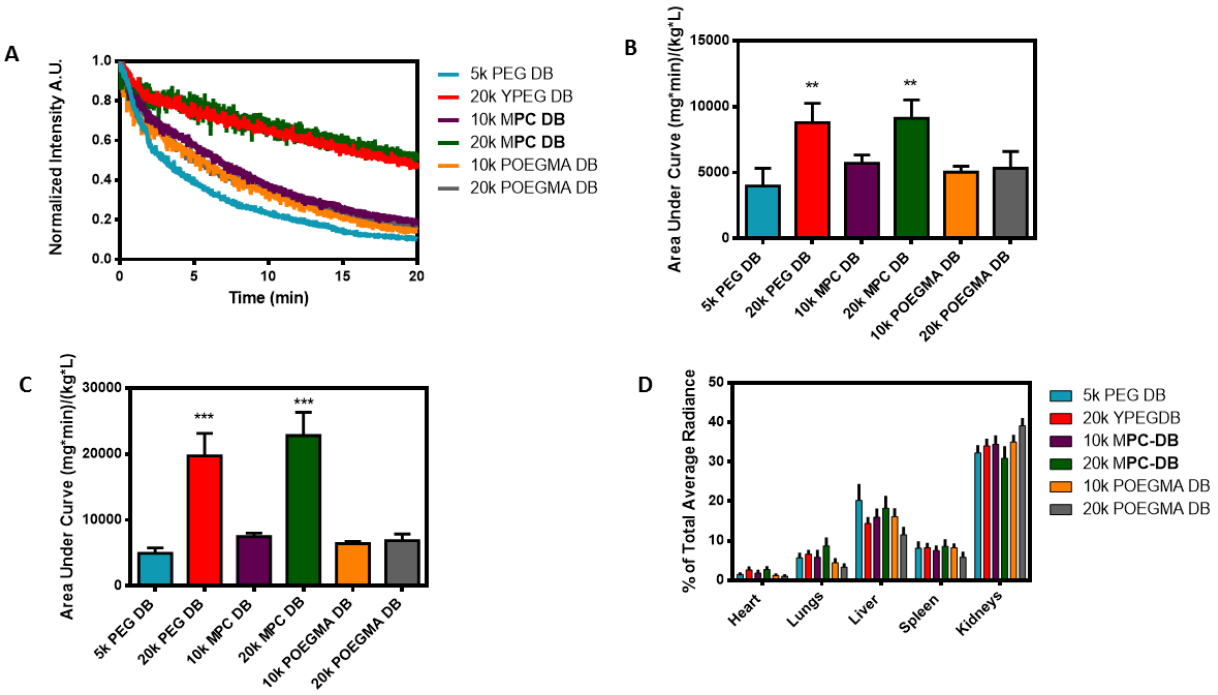

Figure 7: **In vivo *pharmacokinetics and biodistribution.*** *A) Average fluorescence intensity curves from mouse ear recorded for 20 minutes of imaging (n=4). B) Area under curve from t=0 min to t=20 min. C) Area under curve from t=0 min to t= infinitity. 20k PEG DB and 20k MPC DB had significantly improved area under the curves compared to other polyplexes. D) Organ biodistribution at 20 minutes for all polyplexes.*

Polymer	T ½ (min)	AUC (mg *min)/(kg*L)	Cl (mL/min)
PEG DB	5.21 ± 1.66	4952.75 ± 723.11	0.22 ± 0.04
20k PEG DB	22.43 ± 5.80	19734.50 ± 2953.17	0.06 ± 0.01
10k MPC DB	8.44 ± 1.01	7494.00 ± 441.32	0.14 ± 0.01
20k MPC DB	26.28 ± 5.45	22817.5 ± 3048.12	0.05 ± 0.01
10k POEGMA DB	7.61 ± 0.37	6427 ± 274.27	0.16 ± 0.01
20k POEGMA DB	7.42 ± 1.96	6886.25 ± 876.78	0.16 ± 0.023

Table 3: Pharmacokinetic Parameters. *Quantification of pharmacokinetic parameters based on analysis from Graphpad Prism. 20k PEG DB and 20k MPC DB had superior pharmacokinetic properties to other polyplexes.*

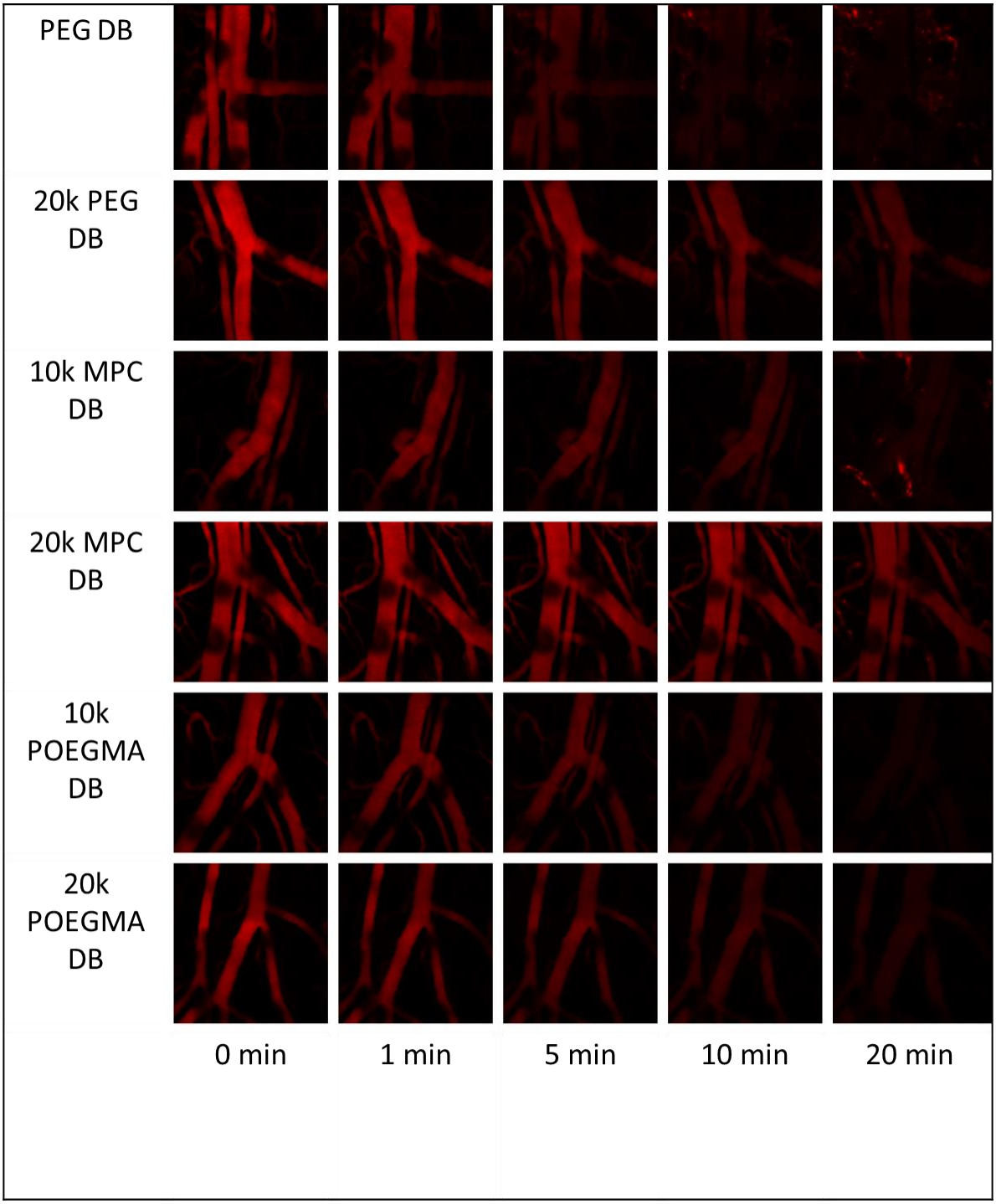

Figure 8: Panel of intravital microscopy images*. Intravital microscopy allows for visualization of pharmacokinetic differences between polyplexes.*

Organ biodistribution data further supported this result (**Figure 7D**). Overall, there was minimal polyplex accumulation in the heart and lungs. All of the novel coronas had slightly decreased accumulation in the liver as compared to traditional linear PEG, which had the lowest average half-life. 20k POEGMA DB, the least stable of the polyplexes, had the highest accumulation in the kidneys, most likely a result of its poor resistance to heparin sulfate. There were no significant differences in the distribution profile between 20k PEG DB and 20k MPC DB. However, the fluorescence from the 20k MPC DB polyplexes is more shifted toward the liver than the kidneys as compared to the 20k PEG DB polyplexes. While the goal of these stealth coronas is to avoid RES uptake, this result may indicate that more of the 20k MPC DB polyplexes stay intact in the blood stream for longer (polyplexes that have fallen apart and released the Cy5 DNA would have more signal in the kidneys due to glomerular filtration). Thus, this result may be promising because if circulation and liver accumulation are increased, this increases the likelihood that tumor accumulation will also increase via the EPR effect. While the % of total fluorescence for the PEG DB appears higher in the liver, overall fluorescence at 20 min was lowest for PEG DB in all organs (**Supplemental Figure S2**), implying that large amounts of these polyplexes had already been eliminated.

In Vivo Tumor Gene Silencing and Biodistribution

It was hypothesized that because of the superior pharmacokinetics of 20k PEG DB and 20k MPC DB, these two polyplex carriers should exhibit improved tumor accumulation and therefore improved gene silencing compared to 5k linear PEG DB carriers. We therefore established luciferase expressing MDA-MB 231 tumors in nude mice and intravenously injected 20k PEG DB, 20k MPC DB, or 5k PEG DB bearing luciferase or scrambled siRNAs. The

animals received a single dose at 1 mg/kg siRNA once tumors had grown to roughly 75 mm^3, and were imaged after luciferin injections on Day 1, 3, 5, 7, and 10 post-injection (**Figure 9A**). The relative luminescence of each individual tumor was compared to its luminescence prior to polyplex injection, and these values were normalized to the average relative luminescence values for the scrambled control polyplexes. There were no significant differences in relative luminescence between any scrambled control polyplex groups, indicating no major tumor toxicity from the carriers alone.

Throughout the 10 day period post-injection, mice treated with 20k MPC DB polyplexes containing luciferase siRNA exhibited potent and robust gene silencing (**Figure 9B**). Throughout the treatment, relative luminescence values for 20k MPC DB averaged about 20% that of scrambled controls. Both 20k PEG DB and 5k PEG DB exhibited lower relative luminescence values compared to their scrambled controls, but the % luminescence of 20k PEG DB was not significantly different from that of PEG DB throughout the study timeline. This study suggests that despite their similar pharmacokinetic properties, 20k MPC DB has superior *in vivo* bioactivity compared to 20k PEG DB.

A few polyplex-related deaths were observed in the tumor-bearing mice that were not previously observed in the pharmacokinetic studies with CD-1 mice. Five mice, all from different polymer treatment groups, died within an hour after polyplex injection. There were no statistically significant differences in survival between polyplex groups (**Figure 9D**). We hypothesize that the high polymer concentration needed for a polyplex N:P ratio of 20 at 1 mg/kg siRNA led to dose-related toxicities. As a result of toxicity concerns, mice body weights were recorded each day during the study period, and there were no significant weight changes or

differences between polyplex treatment groups (**Figure 9C**). Future work is needed to optimize polyplex dose ranges.

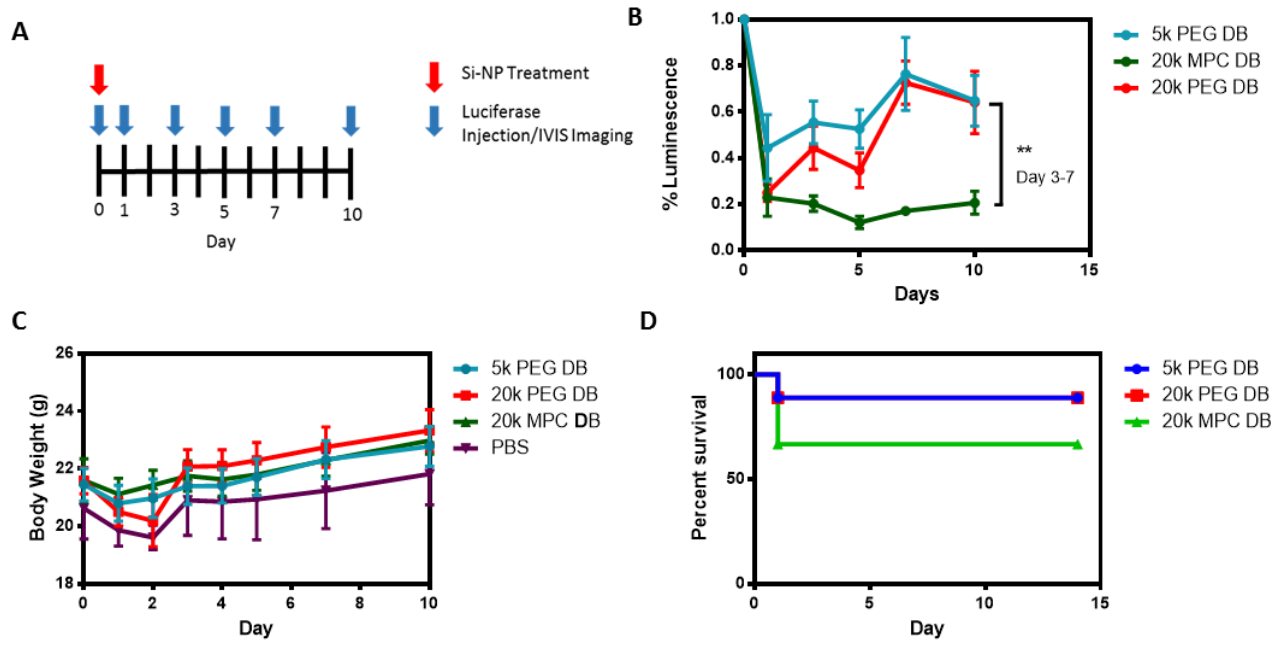

Figure 9: In vivo tumor bioactivity *A) Mice treated once and imaged according to pictured schedule. B) 20k MPC DB had superior in vivo luciferase knockdown properties compared to 5k PEG DB and 20k PEG DB on Days 3-7 (n=6-10 tumors per group), $p<0.05$. C) Mouse body weight measurements indicated no major toxicity from single treatment. D) Overall survival was not significantly different between treatment groups.*

In order to elucidate the mechanism behind the superior tumor gene knockdown of 20k MPC DB, tumor-bearing mice were injected with polyplexes containing Cy5 DNA and sacrificed at either 2 hours or 24 hours. At each of these time points, organs were imaged for fluorescence using in vivo imaging system, and tumors were processed for flow cytometry. Corroborating our previous pharmacokinetic data, organ biodistribution results indicated that at 2 hours, 5k PEG DB was higher in the kidneys, but mostly cleared from circulation by 24 hours.

20k MPC DB and 20k PEGDB fluorescence were much higher than 5k PEG DB in the kidneys at 24 hours, implying a longer blood residence time and slower clearance mechanisms (**Figure 10 A-D**). Interestingly, there were no statistically significant differences in tumor fluorescence between the lead polyplexes at either time point.

Closer analysis of tumor uptake data from flow cytometry data revealed a different story. While there were no significant differences between tumors at 2 hours, at 24 hours there were significantly higher uptake levels for tumors treated with 20k MPC DB compared to those treated with 20k PEG DB or 5k PEG DB (**Figure 11 A, Figure 11C)**. Additionally, up to 90% of GFP-expressing tumor cells were positive for Cy5 signal in the case of 20k MPC DB treatment (**Figure 11B**). 20k PEG DB had the second highest levels of tumoral uptake at around 80% positive, followed by 5k PEG DB at around 40%. These results indicate that zwitterionic MPC-based coronas improve *in vivo* tumor accumulation and uptake as compared to PEG-based coronas. The superior pharmacokinetic properties of both 20k MPC and 20k PEG DB coronas appear to have both increased tumor accumulation relative to traditional 5k PEG DB coronas, but zwitterionic coronas improved overall tumor uptake.

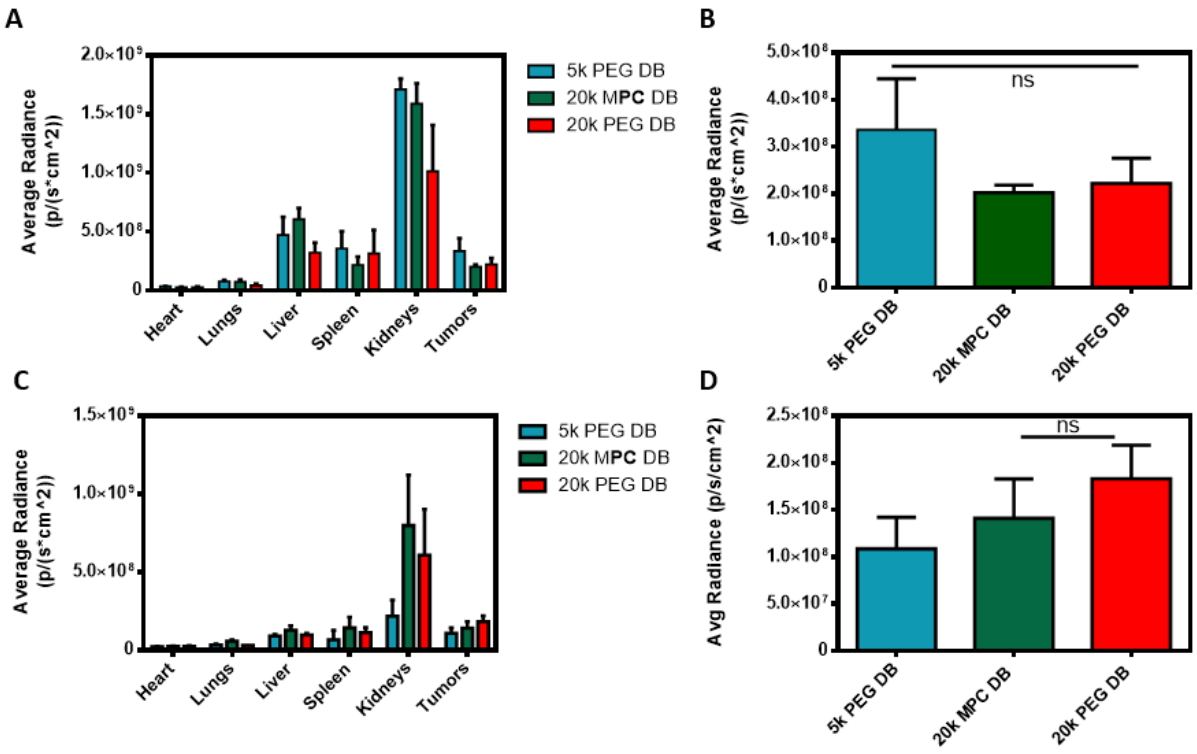

***Figure 10**: **Polyplex Tumor Biodistribution**. A and B) Overall biodistribution at 2 hours shows no significant differences between polyplex tumor accumulation, but increased 5k PEG DB accumulation in the kidneys as compared to at 24 hours. C) Polyplex biodistribution at 24 hours shows increased prescence of 20k MPC DB and 20k PEG DB in kidneys relative to PEG DB. No significant differences between these polyplexes in tumor fluorescence.*

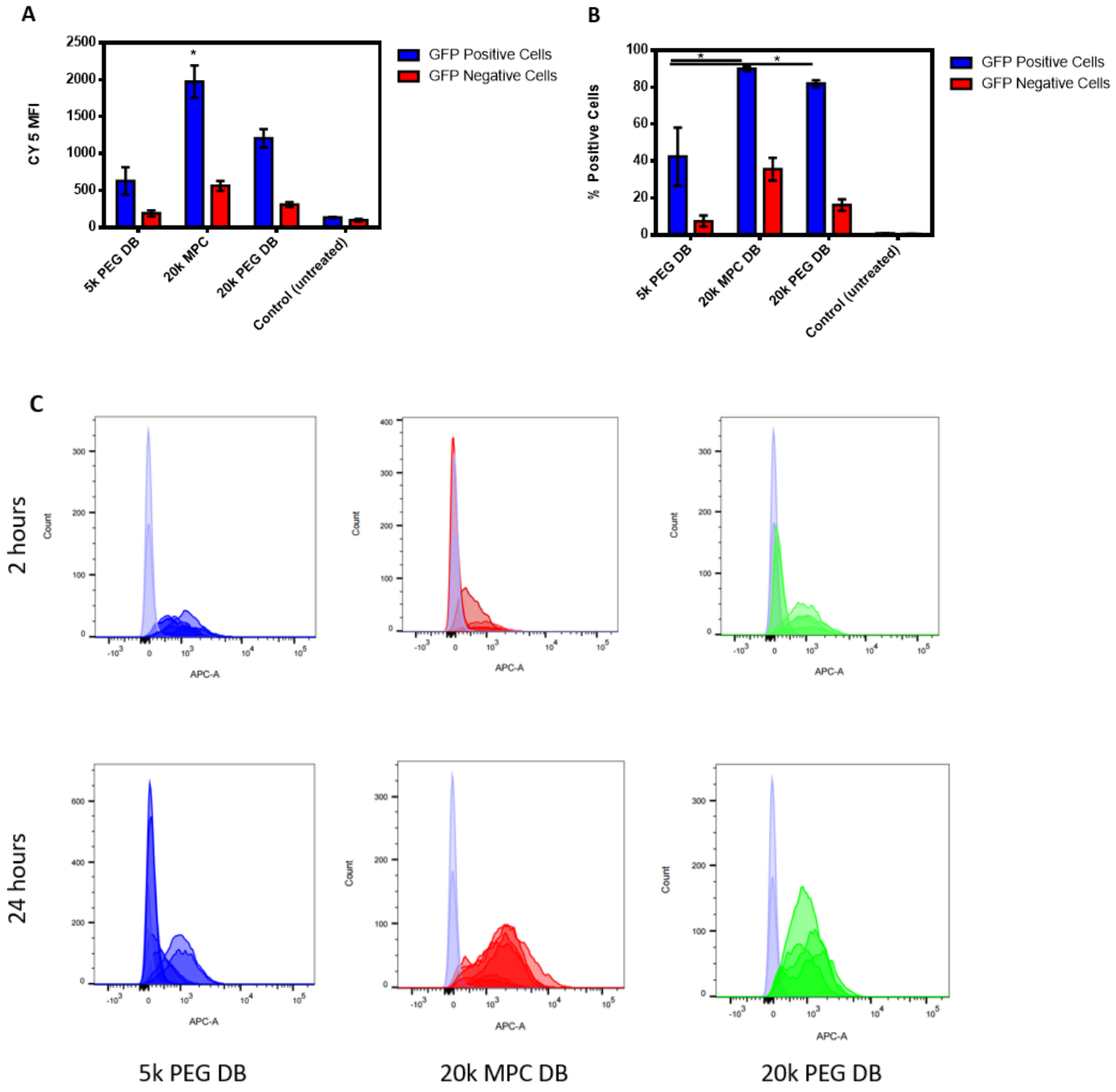

Figure 11: *In Vivo* Tumor Uptake of Polyplexes. *A) 20k MPC DB polyplexes had significantly increased Cy5 fluorescence in tumor cells compared to 20k PEG DB and 5k PEG DB (p=0.0005 for PEG DB diff, p=0.0526 for 20k PEG DB diff., α=0.1). B) Both 20k MPC DB and 20k PEG*

DB had significantly increased % of positive cells compared to 5k PEG DB (α=0.1). C) Raw Cy5 fluorescence data shows no differences between tumor uptake at 2 hours, but larger differences at 24 hours.

Recent work in the field of zwitterionic nanocarriers has described a "switchable" surface charge property of zwitterionic coronas in acidic enviroments, such as that of a tumor.[57] This theory states that if the pH of a tumor microenvironment is low enough, the zwitterionic can become slightly more positively charged than negatively charged, thus facilitating cellular uptake. This phenomenon has not been well-characterized for MPC-based polymers, but our tumor results suggest that further study of these properties is warranted.

CHAPTER IV

CONCLUSION

In this work, we have synthesized and studied 6 unique siRNA polyplex corona chemistries building on previous work that optimized the core forming polymer block. We have shown that high molecular weight coronas composed of either PEG or zwitterionic MPC improve polyplex stability, resist protein adsorption, and significantly enhance intravenous polyplex pharmacokinetics over carriers containing lower molecular weight PEG and MPC. Additionally, we have demonstrated that polyplexes containing brush-like PEG chains (POEGMA) do not significantly improve pharmacokinetic properties over traditional linear PEG. We utilized high resolution intravital microscopy to characterize these pharmacokinetic parameters and to thoroughly compare zwitterionic to PEG-based coronas, a comparison that has not yet been made in the context of *in vivo* siRNA polyplex properties. Finally, we discovered that while there were few pharmacokinetic differences between 20k PEG and 20k MPC coronas, the zwitterionic coronas significantly improved *in vivo* luciferase silencing through superior tumor accumulation and tumor cell uptake properties. This work has important implications for optimization of siRNA nanocarriers used for systemic cancer therapeutics. Additionally, our findings are broadly applicable to the field of drug delivery science for optimization of nanomaterials to improve their efficacy in cancer-related applications.

CHAPTER V

MATERIALS and METHODS

Materials

All materials were purchased from Sigma Aldrich unless otherwise described. Inhibitors were removed from dimethylaminoethyl methacrylate (DMAEMA) and buty methacrylate (BMA) using an activated aluminum oxide column. All DNA or siRNA oligonucleotides were purchased from Integrated DNA Technologies (Coralville, IA, USA).

Polymer Synthesis

All polymers were synthesized using 4-cyano-4-(ethylsulfanylthiocarbonyl)sulfanylpentanoic acid (ECT) as an initial chain transfer agent. ECT was synthesized in house according to previously published methods.[62] PEG DB was synthesized as previously described by coupling a 5 kDa hydroxyl-terminated PEG (JenKem, USA) to ECT by DCC DMAP coupling. ECT was added to the 5 KDa PEG at a 10:1 molar ratio. Dicyclohexyl carbodiimide (DCC) and 4-dimethylaminopyridine (DMAP) were added at 5 molar equivalents the amount of PEG. The coupling reaction was stirred at room temperature for 48 hours and the final product was purified as previously described.[62] From the 5 kDa PEG macroCTA, DMAEMA and BMA were RAFT polymerized at 50:50 molar ratios using AIBN as an initiator (10:1 CTA:Initiator ratio) in 10% w/v dioxane. Reactions were planned with an aimed degree of polymerization of 240, in order to achieve 75-80 repeating units each of DMAEMA and BMA (at a 65-70% monomer conversion rate). The reaction was nitrogen purged for 30 minutes and then was stirred at 65 ˚C for 24 hours. The final reaction mixture was dialyzed into methanol, then water, and lyophilized. 20k

PEG DB was synthesized using the same methods as for the 5k PEG DB polymers, but a 20kDa Y-shaped hydroxyl PEG (JenKem, Plano TX, USA) was conjugated to ECT to create the appropriate macroCTA. Zwitterionic MPC DB was synthesized in a two step process. First, DMAEMA and BMA were RAFT polymerized at the same monomer feed ratios and conversion estimates described above. 1H NMR was used to evaluate conversion rate. This random DMAEMA-BMA copolymer (DB ECT) was then used as a macroCTA to polymerize a homopolymer block of 2-(methacryoyloxyethyl) phosphorylcholine. For a 20,000 kDa corona or a 10, 000 kDa corona, target degree of polymerizations of 75 and 40 were used respectively. These polymerizations used AIBN at a 5:1 CTA: initiator ratio and 10% w/v anhydrous methanol. Reactions were purged with nitrogen for 30 minutes before heating to 65 ˚C for 24 hours. Final reaction products were dialyzed in methanol, then water, and lyophilized. Polymers with POEGMA (poly(ethylene glycol) ethyl ether methacrylate) (Mn =950) in the corona were synthesized in a similar method, but using a 10:1 CTA:initiator ratio and dioxane as a reaction solvent.. Prior to polymerization, inhibitors were removed from POEGMA monomers by first dissoving in anhydrous THF, running through an alumna column, and then drying using a rotovap system. Lower monomer conversion rates of 40-50% were achieved with POEGMA monomers, so aimed degrees of polymerization were adjusted accordingly.

All polymers were characterized using 1H nuclear magnetic resonance spectroscopy (Bruker, 400 MHz). Polymer polydispersity was evaluated with DMF mobile phase gel permeation chromatography (GPC, Agilent Technologies, CA). All NMR spectra are shown in **Supplemental Figure S1**.

Polyplex Formation and Encapsulation Efficiency

All polyplexes in this work were first complexed with siRNA in 10 mM or 100 mM citrate buffer at pH4, allowed to sit for 30 minutes, and then the pH was raised to 7.4 using pH 8 phosphate buffer at 5x the volume of the pH 4 solution. Polyplexes encapsulation efficiency at various N:P ratios was evaluated using a Quant -iT Ribogreen assay kit (ThermoFisher, USA). Assay solutions were prepared based on manufacturer's instructions, and Ribogreen fluorescence was measured using the high range assay. Polyplex solutions were prepared at 100 nM siRNA, and 50 uL of polyplex solution was diluted by half in 1X TE buffer, followed by addition of 100 uL Ribogreen reagent to each well. Fluorescence was measured at 520 nm and encapsulation efficiency was calculated by normalizing fluorescence of polyplex solutions to fluorescence of siRNA-only control solutions.

Polyplex Stability Evaluations

Polyplex diameters and zeta potentials were measured using dynamic light scattering (Zetasizer Nano ZS, Malvern Instruments, Westborough, MA). For these measurements, polyplexes were prepared at final concentrations of 0.167 mg/mL. For stability measurements, each polyplex solution was incubated with 0.1 or 0.25 M NaCl solutions. Salt solutions made up 20% or less of the total solution volume to avoid significant pH changes.

Polyplex stability was also measured in FBS and heparan sulfate through a FRET assay described previously.[33, 62, 70] Briefly, polyplexes were co-loaded with DNAs conjugated with either Alexa Fluor 488 or Alexa Fluor -546 dyes , forming Forster resonance energy transfer pairs. Intensity of fluorescence emission after excitation at 488 nm was measured at 514 and 572

nm, evaluated using a fluorescence plate reader (Tean Infinite F500, Mannedorf, Switzerland). % FRET for each polyplex sample was calculated as:

$$\frac{I_{572}}{I_{572} + I_{514}}$$

For FBS-based FRET challenge, polyplexes were incubated at concentrations of 100 nM siRNA per well with 10, 20, 40, 40, or 50% FBS. FRET signal of polyplexes incubated with FBS was compared to that of polyplexes in PBS alone. In all cases, black, clear bottom 96 well plates were used for fluorescence measurements. FRET signal was tracked over the course of 100 minutes at 5 minute intervals.

Polyplex stability was also evaluate in response to heparin salts. Again, polyplexes were prepared to have final concentrations of 100 nM siRNA per well. In each well, 90 uL of polyplexes were incubated with 10 uL of various concentrations of heparin salts, ranging from 2 U/mL to 100 U/mL final per well concentrations. FRET signal was then evaluated similarly to the above FBS-based method.

Hemolysis Assay

Red blood cell hemolysis assay was performed using methods described previously.[65] Blood was drawn from consenting human donors according to an IRB-approved protocol. In short, red blood cells (RBCs) were isolated from whole blood and diluted into buffer solutions of pH 5.6, 6.2, 6.8, and 7.4. Polyplexes were prepared at 1, 5 and 40 ug/mL polymer and were incubated with red blood cells at the various pH values for 1 hour in round-bottom 96 well plates. Negative controls and positive controls of red blood cells in buffer only or Triton-X, respectively, were also used for analysis. The RBCs were then centrifuged and supernatants were

analyzed for absorbance at 450 nm using a plate reader. Percent hemolysis was evaluated by subtracting background buffer-only RBC absorbance and normalizing to Triton-X controls.

Production of stable luciferase-expressing MDA-MB-231 breast cancer cells and luciferase-expressing NIH 3T3 Mouse fibroblast cells

Lentivirus was produced by transfecting HEK-293T cells with pGreenFire1-CMV plasmid, along with pMDLg/pRRE, pRSV-Rev, and pMD2.G packaging plasmids with Lipofectamine 2000 as a transfection reagent. Media supernatant containing lentivirus was then collected at 48 and 72 hours. For transfection of MDA-MB-231 and NIH-3T3 cell lines, lentiviral media was added to the cells containing 6 ug/mL poybrene for 24 hours of incubation. Cells were analyzed post-transduction by detection of GFP using flow cytometry (BD LSR II Flow Cytometer, San Jose, CA, USA). Cells were selected for vector expression by growing in puromycin-containing media.

Cell Culture

All cells used for this manuscript were cultured in Dulbecco's modified Egle's medium (DMEM, Gibco Cell Culture, Carlsbad, CA), containing 4.5 g/L glucose, 10 % fetal bovine serum (Gibco), and 0.1% gentamicin (Gibco).

Cell Viability

Luciferase-expressing NIH 3T3 cells were seeded in a 96-well plate at 20,000 cells/mL (2000 cells per well). After 24 hours, polyplex solutions were introduced to the wells using an N:P ratio of 20 along with 100 nM scrambled siRNA per well. After 24 hours, polyplex-

containing media was removed from the cells and replaced with media containing luciferin substrate (150 ug/mL). After incubating for 5 minutes, cells were imaged using an IVIS Lumina III imaging system (Caliper Life Sciences, Hopkinton, Massachusetts). Luciferin-containing media was then replaced with normal media for 24 more hours, followed by another round of IVIS imaging with luciferin media at 48 hours. Luminescence signal was compared to untreated controls for analysis.

***In vitro* luciferase silencing of MDA-MB 231 cells**

Luciferase-expressing MDA-MB 231 cells were seeded in 96 well plates at 2000 cells per well and allowed to grow for 24 hours. Polyplex solutions containing either luciferase siRNA or scrambled siRNA at 100 nM were then incubated with MDA-MB 231 cells in quadruplicate. After 24 hours, media was replaced with luciferin-containing media (150 ug/mL) and luminescence was evaluated by IVIS imaging. Luciferin-containing media was then replaced with normal media until 48 hours, at which point luciferin media was reintroduced, and luminescence again evaluated. For analysis of knockdown, all data were normalized to scrambled control polyplexes to account for any toxicity effects.

Uptake by MDA-MB 231 cells

Non-luciferase expressing MDA-MB-231 cells were seeded in 12-well plates at 80,000 cells per well. Polyplexes were formed containing 100 nM of Alexa Fluor 488-conjugated DNA in complete media. After 24 hours, polyplex-containing media was removed. Cells were washed with PBS, trypsinized for 10 minutes in 0.25% trypsin, and centrifuged at 450 xg for 7 min. Cell pellets were then resuspended in PBS containing 0.04% trypan blue (to quench extracellular fluorescence) just prior to adding them to a flow cytometer (FACSCalibur, BD Biosciences, Franklin Lakes, MJ, USA). Cells were monitored for AlexaFluor 488 fluorescence at excitation

and emission wavelengths of 488 and 519 nmn, respectively. Quantification of % uptake was performed using FlowJo software (FlowJo, LLC, Ashland, OR). Untreated MDA-MB 231 cells were used as negative controls.

Isothermal Titration Calorimetry

Isothermal Titration Calorimetry experiments were performed using a MicroCal VP-ITC (Malvern, USA) in the Vanderbilt Center for Structural Biology Core. Polyplexes were prepared at concentrations of 0.5 mg/mL polymer as described above. Bovine Serum Albumin (BSA) was dissolved from lyophilized powder at 15 mg/mL in buffer solutions exactly matching the composition of polyplex buffer. Titration experiments were carried out at 37 ºC using a reference power of 10 ucal/ sec, 300 second initial delay, 307 rpm stirring speed. Each injection was 10 uL, with a duration of 20 sec, spacing of 260 seconds, and filter period of 2 seconds. A control consisting of heat of dilution of BSA into buffer only was subtracted from titration data. All data analysis was performed in Origin, using a one set of sites binding model to determine thermodynamic parameters. A cationic control polymer consisting of DMAEMA only in the corona, as previously described[33], was used as a positive control for protein adsorption.

Complement Assay

All materials for the hemolysis-based complement assay were purchased from Complement Technologies (Tyler, TX, USA). siRNA polyplexes were prepared at 50 nM siRNA. Complement sera was prepared at five dilutions (1:20, 1:40, 1:80, 1:160, 1:320), and was then Antibody-sensitized sheep red blood cells were prepared at 2x 10^8 cells/mL in GVB $^{++}$ buffer. In each test tube, 10 0uL of complement sera was added to 100 uL pof polyplexes and incubated for 30 minutes. Then 100 uL of antibody-sensitized RBCs were added to each tube and the mixtures were incubated at 37 ºC for 1 hour with intermittent shaking. All samples were then

centrifuged and supernatants were transferred to a 96 well plate. Absorbance at 541 nm was then measured on a plate reader. Absorbance values were used to determine transmittance and absorption (1-transmittance). Percent lysis was calculated by subtracting absorption of PBS/RBC only controls from sample absorption and dividing by absorption for complete lysis controls (water+RBCs) minus absorption of PBS/RBC controls. Percent lysis at each complement dilution was plotted and compared to control samples containing complement proteins only (no polyplexes).

Polyplex pharmacokinetics, biodistribution, and intravital microscopy

In vivo polyplex preparation

For *in vivo* polyplex preparations, polymers were complexed with 1 mg/kg Cy5-conjugated DNA olignonucleotides in 100 mM pH4 citrate buffer. Complexing solutions were then loaded into 20 kDa MWCO dialysis tubing (Spectrum Laboratories, Rancho Dominguez, CA) and dialyzed into PBS -/- overnight. Polyplex formation was confirmed by dynamic light scattering (described above) immediately prior to *in vivo* injections.

Intravital microscopy

Male CD-1 mice (Charles River) (n=4 per group), were anesthetized using isoflurane and immobilized on heated confocal microscope stage. Prior to imaging, mouse ears were naired. Microscope immersion fluid was used to immobilize the mouse ear on a glass coverslip. Intravital microscopy was performed using a Nikon Czsi+ system with a Nikon Eclipse Ti-oE inverted microscopy base, Plan ApoVC 20x differential interference contrast N2 objective, 0.75 NA, Galvano scanner, and 543 dichroic mirror. All image analysis and acquisition was done using Nikon NIS-Elements AR version 4.30.01. A laser power of 98 was used throughout. Ear veins were detected using the light microscope and images were focused to the plane of greatest

vessel width, where flowing red blood cells were clearly visible. Once the ear was in focus, microscope was switched to confocal laser mode and set to image continuously every second. The mouse was then injected with 100 uL polyplex solution via tail vein at a 1 mg/kg dose, and Cy5 fluorescence in ear veins was monitored for 20 minutes. For image analysis, initial background fluorescence was subtracted, and circular regions of interest were highlighted within the mouse ear vessels. Fluorescence from these regions of interest was quantified and background fluorescence was subtracted. Intensity values were normalized to initial peak intensity. Fluorescence decay curves were modeled as one-compartment systems using single phase exponential decay. Pharmacokinetic parameters were calculated using Graphpad Prism analysis software.

Biodistribution

After 20 min of monitoring via intravital microscopy, animals were sacrificed. Organs were removed and immediately imaged for Cy5 fluorescence using an IVIS system. Fluorescence was quantified using an IVIS Lumina Imaging system (Xenogen Corporation, Alameda, CA, USA) at excitation and emission wavelengths of 620 and 670 nm, respectively.

In Vivo Tumor Gene Silencing

Athymic female nude mice (4-6 weeks old, Jackson Laboratory) were injected in the mammary fatpad on each side with 1 x 10^6 Luciferase expressing MDA-MB-231 cells in a 50:50 mixture of Matrigel:DMEM (serum-free). Tumor growth was followed until they reached approximately 75 mm^3. Polyplexes were prepared bearing either luciferase or scrambled siRNA at 1 mg/kg as described for pharmacokinetic studies. Animals were injected i.p. with luciferin

substrate (150mg/kg) imaged for baseline tumor luminescence using an IVIS system, and then were subsequently injected with polyplexes via tail vein. Mice were re-injected with luciferin substrate on Days 1, 3, 5, 7, and 10 post-treatment. Luminescence signal of each individual tumor was compared to its baseline pre-treatment signal, and each relative luminescence value was normalized to the average relative luminescence of respective scrambled siRNA polyplex groups (n=6-10 tumors per group). Body weight measurements of all mice were recorded every day of the study period to note any signs of toxicity.

Biodistribution of Tumor Bearing Mice

Biodistribution studies for athymic female nude tumor-bearing mice (Jackson Laboratory) were conducted using the same methods as biodistribution studies for the male CD-1 mice. All polyplexes were similarly loaded with Cy5 conjugated DNA and fluorescence was measured in heart, lungs, kidneys, liver, spleen, and tumors. Organs were excised at 2 hour and 24-hour time points post tail vein injection.

In Vivo Polyplex Uptake by MDA-MB-231 breast tumors

Tumors isolated from mice during above-described biodistribution experiments were then used for flow cytometry studies of polyplex uptake. Tumors were cut into small pieces, washed with HBSS containing Ca and Mg, and then processed using an enzyme mix containing collagenase (0.5 mg/mL, Roche Life Sciences, Indianapolis, IN, USA) and DNAse (0.19 mg/mL, BioRAD, Hercules, CA, USA) in DMEM. After 1 hour incubation in enzyme mix, the tumors were centrifuged and re-suspended in HBSS without Ca and Mg, and then incubated with 5 mM EDTA for 20 minutes. Tumors were then centrifuged and the pellets were re-suspended in HBSS

with Ca and Mg and filtered using a 70 um Nylon cell strainer. Filtrate was then washed once more with HBSS containing Ca and MG, and then incubated in ACK lysis buffer (Thermo Fisher Scientific, USA) for 2 minutes before being diluted in 20 mL of PBS -/-. Cells were then pelleted and re-suspended in 1-2 mL PBS-/- prior to running on a flow cytometer (BD LSRii, BD Biosciences, San Jose, CA, USA). Uptake analysis was performed in FlowJo.

REFERENCES

1. Fire, A.; Xu, S.; Montgomery, M. K.; Kostas, S. A.; Driver, S. E.; Mello, C. C., Potent and specific genetic interference by double-stranded RNA in Caenorhabditis elegans. *Nature* **1998,** *391* (6669), 806-811.

2. Wang, J.; Lu, Z.; Wientjes, M. G.; Au, J. L., Delivery of siRNA therapeutics: barriers and carriers. *Aaps j* **2010,** *12* (4), 492-503.

3. Ozcan, G.; Ozpolat, B.; Coleman, R. L.; Sood, A. K.; Lopez-Berestein, G., Preclinical and clinical development of siRNA-based therapeutics. *Advanced Drug Delivery Reviews* **2015,** *87*, 108-119.

4. Coelho, T.; Adams, D.; Silva, A.; Lozeron, P.; Hawkins, P. N.; Mant, T.; Perez, J.; Chiesa, J.; Warrington, S.; Tranter, E.; Munisamy, M.; Falzone, R.; Harrop, J.; Cehelsky, J.; Bettencourt, B. R.; Geissler, M.; Butler, J. S.; Sehgal, A.; Meyers, R. E.; Chen, Q.; Borland, T.; Hutabarat, R. M.; Clausen, V. A.; Alvarez, R.; Fitzgerald, K.; Gamba-Vitalo, C.; Nochur, S. V.; Vaishnaw, A. K.; Sah, D. W.; Gollob, J. A.; Suhr, O. B., Safety and efficacy of RNAi therapy for transthyretin amyloidosis. *N Engl J Med* **2013,** *369* (9), 819-29.

5. Whitehead, K. A.; Langer, R.; Anderson, D. G., Knocking down barriers: advances in siRNA delivery. *Nat Rev Drug Discov* **2009,** *8* (2), 129-138.

6. Czauderna, F.; Fechtner, M.; Dames, S.; Aygün, H.; Klippel, A.; Pronk, G. J.; Giese, K.; Kaufmann, J., Structural variations and stabilising modifications of synthetic siRNAs in mammalian cells. *Nucleic Acids Research* **2003,** *31* (11), 2705-2716.

7. Juliano, R.; Alam, M. R.; Dixit, V.; Kang, H., Mechanisms and strategies for effective delivery of antisense and siRNA oligonucleotides. *Nucleic Acids Research* **2008,** *36* (12), 4158-4171.

8. Kim, D. H.; Rossi, J. J., Strategies for silencing human disease using RNA interference. *Nat Rev Genet* **2007,** *8* (3), 173-184.

9. Ozpolat, B.; Sood, A. K.; Lopez-Berestein, G., Nanomedicine based approaches for the delivery of siRNA in cancer. *J Intern Med* **2010,** *267* (1), 44-53.

10. Zuckerman, J. E.; Davis, M. E., Clinical experiences with systemically administered siRNA-based therapeutics in cancer. *Nat Rev Drug Discov* **2015,** *14* (12), 843-856.

11. Matsuda, S.; Keiser, K.; Nair, J. K.; Charisse, K.; Manoharan, R. M.; Kretschmer, P.; Peng, C. G.; A, V. K. i.; Kandasamy, P.; Willoughby, J. L.; Liebow, A.; Querbes, W.; Yucius, K.; Nguyen, T.; Milstein, S.; Maier, M. A.; Rajeev, K. G.; Manoharan, M., siRNA Conjugates Carrying Sequentially Assembled Trivalent N-Acetylgalactosamine Linked Through

Nucleosides Elicit Robust Gene Silencing In Vivo in Hepatocytes. *ACS Chem Biol* **2015,** *10* (5), 1181-7.

12. Rajeev, K. G.; Nair, J. K.; Jayaraman, M.; Charisse, K.; Taneja, N.; O'Shea, J.; Willoughby, J. L.; Yucius, K.; Nguyen, T.; Shulga-Morskaya, S.; Milstein, S.; Liebow, A.; Querbes, W.; Borodovsky, A.; Fitzgerald, K.; Maier, M. A.; Manoharan, M., Hepatocyte-specific delivery of siRNAs conjugated to novel non-nucleosidic trivalent N-acetylgalactosamine elicits robust gene silencing in vivo. *Chembiochem* **2015,** *16* (6), 903-8.

13. Yasuda, M.; Gan, L.; Chen, B.; Kadirvel, S.; Yu, C.; Phillips, J. D.; New, M. I.; Liebow, A.; Fitzgerald, K.; Querbes, W.; Desnick, R. J., RNAi-mediated silencing of hepatic Alas1 effectively prevents and treats the induced acute attacks in acute intermittent porphyria mice. *Proceedings of the National Academy of Sciences* **2014,** *111* (21), 7777-7782.

14. Nakayama, T.; Butler, J. S.; Sehgal, A.; Severgnini, M.; Racie, T.; Sharman, J.; Ding, F.; Morskaya, S. S.; Brodsky, J.; Tchangov, L.; Kosovrasti, V.; Meys, M.; Nechev, L.; Wang, G.; Peng, C. G.; Fang, Y.; Maier, M.; Rajeev, K. G.; Li, R.; Hettinger, J.; Barros, S.; Clausen, V.; Zhang, X.; Wang, Q.; Hutabarat, R.; Dokholyan, N. V.; Wolfrum, C.; Manoharan, M.; Kotelianski, V.; Stoffel, M.; Sah, D. W., Harnessing a physiologic mechanism for siRNA delivery with mimetic lipoprotein particles. *Mol Ther* **2012,** *20* (8), 1582-9.

15. Bartlett, D. W.; Davis, M. E., Impact of tumor-specific targeting and dosing schedule on tumor growth inhibition after intravenous administration of siRNA-containing nanoparticles. *Biotechnol Bioeng* **2008,** *99* (4), 975-85.

16. Matsumura, Y.; Maeda, H., A new concept for macromolecular therapeutics in cancer chemotherapy: mechanism of tumoritropic accumulation of proteins and the antitumor agent smancs. *Cancer Res* **1986,** *46* (12 Pt 1), 6387-92.

17. Maeda, H.; Tsukigawa, K.; Fang, J., A Retrospective 30 Years After Discovery of the Enhanced Permeability and Retention Effect of Solid Tumors: Next-Generation Chemotherapeutics and Photodynamic Therapy—Problems, Solutions, and Prospects. *Microcirculation* **2016,** *23* (3), 173-182.

18. Maeda, H.; Nakamura, H.; Fang, J., The EPR effect for macromolecular drug delivery to solid tumors: Improvement of tumor uptake, lowering of systemic toxicity, and distinct tumor imaging in vivo. *Adv Drug Deliv Rev* **2013,** *65* (1), 71-9.

19. Prabhakar, U.; Maeda, H.; Jain, R. K.; Sevick-Muraca, E. M.; Zamboni, W.; Farokhzad, O. C.; Barry, S. T.; Gabizon, A.; Grodzinski, P.; Blakey, D. C., Challenges and key considerations of the enhanced permeability and retention (EPR) effect for nanomedicine drug delivery in oncology. *Cancer research* **2013,** *73* (8), 2412-2417.

20. Bertrand, N.; Leroux, J. C., The journey of a drug-carrier in the body: an anatomo-physiological perspective. *J Control Release* **2012,** *161* (2), 152-63.

21. Nichols, J. W.; Bae, Y. H., Odyssey of a cancer nanoparticle: From injection site to site of action. *Nano Today* **2012,** *7* (6), 606-618.

22. Alexis, F.; Pridgen, E.; Molnar, L. K.; Farokhzad, O. C., Factors Affecting the Clearance and Biodistribution of Polymeric Nanoparticles. *Molecular Pharmaceutics* **2008,** *5* (4), 505-515.

23. Naeye, B.; Deschout, H.; Caveliers, V.; Descamps, B.; Braeckmans, K.; Vanhove, C.; Demeester, J.; Lahoutte, T.; De Smedt, S. C.; Raemdonck, K., In vivo disassembly of IV administered siRNA matrix nanoparticles at the renal filtration barrier. *Biomaterials* **2013,** *34* (9), 2350-2358.

24. Zuckerman, J. E.; Choi, C. H.; Han, H.; Davis, M. E., Polycation-siRNA nanoparticles can disassemble at the kidney glomerular basement membrane. *Proc Natl Acad Sci U S A* **2012,** *109* (8), 3137-42.

25. Pelaz, B.; del Pino, P.; Maffre, P.; Hartmann, R.; Gallego, M.; Rivera-Fernández, S.; de la Fuente, J. M.; Nienhaus, G. U.; Parak, W. J., Surface Functionalization of Nanoparticles with Polyethylene Glycol: Effects on Protein Adsorption and Cellular Uptake. *ACS Nano* **2015,** *9* (7), 6996-7008.

26. Owens Iii, D. E.; Peppas, N. A., Opsonization, biodistribution, and pharmacokinetics of polymeric nanoparticles. *Int J Pharm* **2006,** *307* (1), 93-102.

27. Nagayama, S.; Ogawara, K.; Fukuoka, Y.; Higaki, K.; Kimura, T., Time-dependent changes in opsonin amount associated on nanoparticles alter their hepatic uptake characteristics. *Int J Pharm* **2007,** *342* (1-2), 215-21.

28. Walkey, C. D.; Olsen, J. B.; Guo, H.; Emili, A.; Chan, W. C. W., Nanoparticle Size and Surface Chemistry Determine Serum Protein Adsorption and Macrophage Uptake. *Journal of the American Chemical Society* **2012,** *134* (4), 2139-2147.

29. Aggarwal, P.; Hall, J. B.; McLeland, C. B.; Dobrovolskaia, M. A.; McNeil, S. E., Nanoparticle interaction with plasma proteins as it relates to particle biodistribution, biocompatibility and therapeutic efficacy. *Advanced Drug Delivery Reviews* **2009,** *61* (6), 428-437.

30. Gref, R.; Lück, M.; Quellec, P.; Marchand, M.; Dellacherie, E.; Harnisch, S.; Blunk, T.; Müller, R. H., 'Stealth' corona-core nanoparticles surface modified by polyethylene glycol (PEG): influences of the corona (PEG chain length and surface density) and of the core composition on phagocytic uptake and plasma protein adsorption. *Colloids and Surfaces B: Biointerfaces* **2000,** *18* (3–4), 301-313.

31. Perry, J. L.; Reuter, K. G.; Kai, M. P.; Herlihy, K. P.; Jones, S. W.; Luft, J. C.; Napier, M.; Bear, J. E.; DeSimone, J. M., PEGylated PRINT Nanoparticles: The Impact of PEG Density on Protein Binding, Macrophage Association, Biodistribution, and Pharmacokinetics. *Nano Letters* **2012,** *12* (10), 5304-5310.

32. Gao, H.; Liu, J.; Yang, C.; Cheng, T.; Chu, L.; Xu, H.; Meng, A.; Fan, S.; Shi, L., The impact of PEGylation patterns on the in vivo biodistribution of mixed shell micelles. *Int J Nanomedicine* **2013,** *8*, 4229-46.

33. Miteva, M.; Kirkbride, K. C.; Kilchrist, K. V.; Werfel, T. A.; Li, H.; Nelson, C. E.; Gupta, M. K.; Giorgio, T. D.; Duvall, C. L., Tuning PEGylation of mixed micelles to overcome intracellular and systemic siRNA delivery barriers. *Biomaterials* **2015,** *38*, 97-107.

34. Zhang, Y.; Xiao, C.; Ding, J.; Li, M.; Chen, X.; Tang, Z.; Zhuang, X., A comparative study of linear, Y-shaped and linear-dendritic methoxy poly(ethylene glycol)-block-polyamidoamine-block-poly(l-glutamic acid) block copolymers for doxorubicin delivery in vitro and in vivo. *Acta Biomater* **2016,** *40*, 243-53.

35. Sato, A.; Choi, S. W.; Hirai, M.; Yamayoshi, A.; Moriyama, R.; Yamano, T.; Takagi, M.; Kano, A.; Shimamoto, A.; Maruyama, A., Polymer brush-stabilized polyplex for a siRNA carrier with long circulatory half-life. *Journal of Controlled Release* **2007,** *122* (3), 209-216.

36. Venkataraman, S.; Ong, W. L.; Ong, Z. Y.; Joachim Loo, S. C.; Rachel Ee, P. L.; Yang, Y. Y., The role of PEG architecture and molecular weight in the gene transfection performance of PEGylated poly(dimethylaminoethyl methacrylate) based cationic polymers. *Biomaterials* **2011,** *32* (9), 2369-2378.

37. Kunath, K.; von Harpe, A.; Petersen, H.; Fischer, D.; Voigt, K.; Kissel, T.; Bickel, U., The Structure of PEG-Modified Poly(Ethylene Imines) Influences Biodistribution and Pharmacokinetics of Their Complexes with NF-κB Decoy in Mice. *Pharmaceutical Research* **2002,** *19* (6), 810-817.

38. Verbaan, F. J.; Oussoren, C.; Snel, C. J.; Crommelin, D. J. A.; Hennink, W. E.; Storm, G., Steric stabilization of poly(2-(dimethylamino)ethyl methacrylate)-based polyplexes mediates prolonged circulation and tumor targeting in mice. *The Journal of Gene Medicine* **2004,** *6* (1), 64-75.

39. Tockary, T. A.; Osada, K.; Chen, Q.; Machitani, K.; Dirisala, A.; Uchida, S.; Nomoto, T.; Toh, K.; Matsumoto, Y.; Itaka, K.; Nitta, K.; Nagayama, K.; Kataoka, K., Tethered PEG Crowdedness Determining Shape and Blood Circulation Profile of Polyplex Micelle Gene Carriers. *Macromolecules* **2013,** *46* (16), 6585-6592.

40. Moghimi, S. M.; Szebeni, J., Stealth liposomes and long circulating nanoparticles: critical issues in pharmacokinetics, opsonization and protein-binding properties. *Progress in Lipid Research* **2003,** *42* (6), 463-478.

41. Chen, H.; Kim, S.; He, W.; Wang, H.; Low, P. S.; Park, K.; Cheng, J. X., Fast release of lipophilic agents from circulating PEG-PDLLA micelles revealed by in vivo forster resonance energy transfer imaging. *Langmuir* **2008,** *24* (10), 5213-7.

42. Mishra, S.; Webster, P.; Davis, M. E., PEGylation significantly affects cellular uptake and intracellular trafficking of non-viral gene delivery particles. *Eur J Cell Biol* **2004,** *83* (3), 97-111.

43. Dams, E. T.; Laverman, P.; Oyen, W. J.; Storm, G.; Scherphof, G. L.; van Der Meer, J. W.; Corstens, F. H.; Boerman, O. C., Accelerated blood clearance and altered biodistribution of repeated injections of sterically stabilized liposomes. *J Pharmacol Exp Ther* **2000,** *292* (3), 1071-9.

44. Ishida, T.; Masuda, K.; Ichikawa, T.; Ichihara, M.; Irimura, K.; Kiwada, H., Accelerated clearance of a second injection of PEGylated liposomes in mice. *Int J Pharm* **2003,** *255* (1-2), 167-74.

45. Ishihara, T.; Takeda, M.; Sakamoto, H.; Kimoto, A.; Kobayashi, C.; Takasaki, N.; Yuki, K.; Tanaka, K.-i.; Takenaga, M.; Igarashi, R.; Maeda, T.; Yamakawa, N.; Okamoto, Y.; Otsuka, M.; Ishida, T.; Kiwada, H.; Mizushima, Y.; Mizushima, T., Accelerated Blood Clearance Phenomenon Upon Repeated Injection of PEG-modified PLA-nanoparticles. *Pharmaceutical Research* **2009,** *26* (10), 2270-2279.

46. Schlenoff, J. B., Zwitteration: Coating Surfaces with Zwitterionic Functionality to Reduce Nonspecific Adsorption. *Langmuir* **2014,** *30* (32), 9625-9636.

47. Amoozgar, Z.; Yeo, Y., Recent advances in stealth coating of nanoparticle drug delivery systems. *Wiley Interdisciplinary Reviews: Nanomedicine and Nanobiotechnology* **2012,** *4* (2), 219-233.

48. Sin, M.-C.; Chen, S.-H.; Chang, Y., Hemocompatibility of zwitterionic interfaces and membranes. *Polym J* **2014,** *46* (8), 436-443.

49. Hayward, J. A.; Chapman, D., Biomembrane surfaces as models for polymer design: the potential for haemocompatibility. *Biomaterials* **1984,** *5* (3), 135-42.

50. Lewis, A. L.; Tolhurst, L. A.; Stratford, P. W., Analysis of a phosphorylcholine-based polymer coating on a coronary stent pre- and post-implantation. *Biomaterials* **2002,** *23* (7), 1697-1706.

51. Bakhai, A.; Booth, J.; Delahunty, N.; Nugara, F.; Clayton, T.; McNeill, J.; Davies, S. W.; Cumberland, D. C.; Stables, R. H., The SV stent study: a prospective, multicentre, angiographic evaluation of the BiodivYsio phosphorylcholine coated small vessel stent in small coronary vessels. *International Journal of Cardiology* **2005,** *102* (1), 95-102.

52. Lewis, A.; Tang, Y.; Brocchini, S.; Choi, J.-w.; Godwin, A., Poly(2-methacryloyloxyethyl phosphorylcholine) for Protein Conjugation. *Bioconjugate Chemistry* **2008,** *19* (11), 2144-2155.

53. Jin, Q.; Chen, Y.; Wang, Y.; Ji, J., Zwitterionic drug nanocarriers: A biomimetic strategy for drug delivery. *Colloids and Surfaces B: Biointerfaces* **2014,** *124*, 80-86.

54. Ishihara, T.; Maeda, T.; Sakamoto, H.; Takasaki, N.; Shigyo, M.; Ishida, T.; Kiwada, H.; Mizushima, Y.; Mizushima, T., Evasion of the Accelerated Blood Clearance Phenomenon by Coating of Nanoparticles with Various Hydrophilic Polymers. *Biomacromolecules* **2010,** *11* (10), 2700-2706.

55. Xiu, K.-M.; Zhao, N.-N.; Yang, W.-T.; Xu, F.-J., Versatile functionalization of gene vectors via different types of zwitterionic betaine species for serum-tolerant transfection. *Acta Biomaterialia* **2013,** *9* (7), 7439-7448.

56. Yu, H.; Zou, Y.; Jiang, L.; Yin, Q.; He, X.; Chen, L.; Zhang, Z.; Gu, W.; Li, Y., Induction of apoptosis in non-small cell lung cancer by downregulation of MDM2 using pH-responsive PMPC-b-PDPA/siRNA complex nanoparticles. *Biomaterials* **2013,** *34* (11), 2738-2747.

57. Zou, H.; Wang, Z.; Feng, M., Nanocarriers with tunable surface properties to unblock bottlenecks in systemic drug and gene delivery. *Journal of Controlled Release* **2015,** *214*, 121-133.

58. Hemp, S. T.; Smith, A. E.; Bryson, J. M.; Allen, M. H.; Long, T. E., Phosphonium-Containing Diblock Copolymers for Enhanced Colloidal Stability and Efficient Nucleic Acid Delivery. *Biomacromolecules* **2012,** *13* (8), 2439-2445.

59. Lomas, H.; Du, J.; Canton, I.; Madsen, J.; Warren, N.; Armes, S. P.; Lewis, A. L.; Battaglia, G., Efficient Encapsulation of Plasmid DNA in pH-Sensitive PMPC–PDPA Polymersomes: Study of the Effect of PDPA Block Length on Copolymer–DNA Binding Affinity. *Macromolecular Bioscience* **2010,** *10* (5), 513-530.

60. Ukawa, M.; Akita, H.; Masuda, T.; Hayashi, Y.; Konno, T.; Ishihara, K.; Harashima, H., 2-Methacryloyloxyethyl phosphorylcholine polymer (MPC)-coating improves the transfection activity of GALA-modified lipid nanoparticles by assisting the cellular uptake and intracellular dissociation of plasmid DNA in primary hepatocytes. *Biomaterials* **2010,** *31* (24), 6355-62.

61. Ahmed, M.; Bhuchar, N.; Ishihara, K.; Narain, R., Well-Controlled Cationic Water-Soluble Phospholipid Polymer−DNA Nanocomplexes for Gene Delivery. *Bioconjugate Chemistry* **2011,** *22* (6), 1228-1238.

62. Nelson, C. E.; Kintzing, J. R.; Hanna, A.; Shannon, J. M.; Gupta, M. K.; Duvall, C. L., Balancing Cationic and Hydrophobic Content of PEGylated siRNA Polyplexes Enhances Endosome Escape, Stability, Blood Circulation Time, and Bioactivity in Vivo. *ACS Nano* **2013,** *7* (10), 8870-8880.

63. Roy, D.; Berguig, G. Y.; Ghosn, B.; Lane, D.; Braswell, S.; Stayton, P. S.; Convertine, A. J., Synthesis and characterization of transferrin-targeted chemotherapeutic delivery systems

prepared via RAFT copolymerization of high molecular weight PEG macromonomers. *Polymer chemistry* **2014,** *5* (5), 1791-1799.

64. Berguig, G. Y.; Convertine, A. J.; Frayo, S.; Kern, H. B.; Procko, E.; Roy, D.; Srinivasan, S.; Margineantu, D. H.; Booth, G.; Palanca-Wessels, M. C.; Baker, D.; Hockenbery, D.; Press, O. W.; Stayton, P. S., Intracellular Delivery System for Antibody–Peptide Drug Conjugates. *Molecular Therapy* **2015,** *23* (5), 907-917.

65. Evans, B. C.; Nelson, C. E.; Yu, S. S.; Beavers, K. R.; Kim, A. J.; Li, H.; Nelson, H. M.; Giorgio, T. D.; Duvall, C. L., Ex Vivo Red Blood Cell Hemolysis Assay for the Evaluation of pH-responsive Endosomolytic Agents for Cytosolic Delivery of Biomacromolecular Drugs. *Journal of Visualized Experiments : JoVE* **2013,** (73), 50166.

66. Bartlett, D. W.; Davis, M. E., Physicochemical and biological characterization of targeted, nucleic acid-containing nanoparticles. *Bioconjugate chemistry* **2007,** *18* (2), 456-468.

67. Huang, R.; Lau, B. L., Biomolecule-nanoparticle interactions: Elucidation of the thermodynamics by isothermal titration calorimetry. (0006-3002 (Print)).

68. Nomoto, T.; Matsumoto, Y.; Miyata, K.; Oba, M.; Fukushima, S.; Nishiyama, N.; Yamasoba, T.; Kataoka, K., In situ quantitative monitoring of polyplexes and polyplex micelles in the blood circulation using intravital real-time confocal laser scanning microscopy. *Journal of Controlled Release* **2011,** *151* (2), 104-109.

69. Jones, S. W.; Roberts, R. A.; Robbins, G. R.; Perry, J. L.; Kai, M. P.; Chen, K.; Bo, T.; Napier, M. E.; Ting, J. P. Y.; DeSimone, J. M.; Bear, J. E., Nanoparticle clearance is governed by Th1/Th2 immunity and strain background. *The Journal of Clinical Investigation 123* (7), 3061-3073.

70. Sarett, S. M.; Werfel, T. A.; Chandra, I.; Jackson, M. A.; Kavanaugh, T. E.; Hattaway, M. E.; Giorgio, T. D.; Duvall, C. L., Hydrophobic interactions between polymeric carrier and palmitic acid-conjugated siRNA improve PEGylated polyplex stability and enhance in vivo pharmacokinetics and tumor gene silencing. *Biomaterials* **2016,** *97*, 122-132.

APPENDIX

SUPPLEMENTAL FIGURES

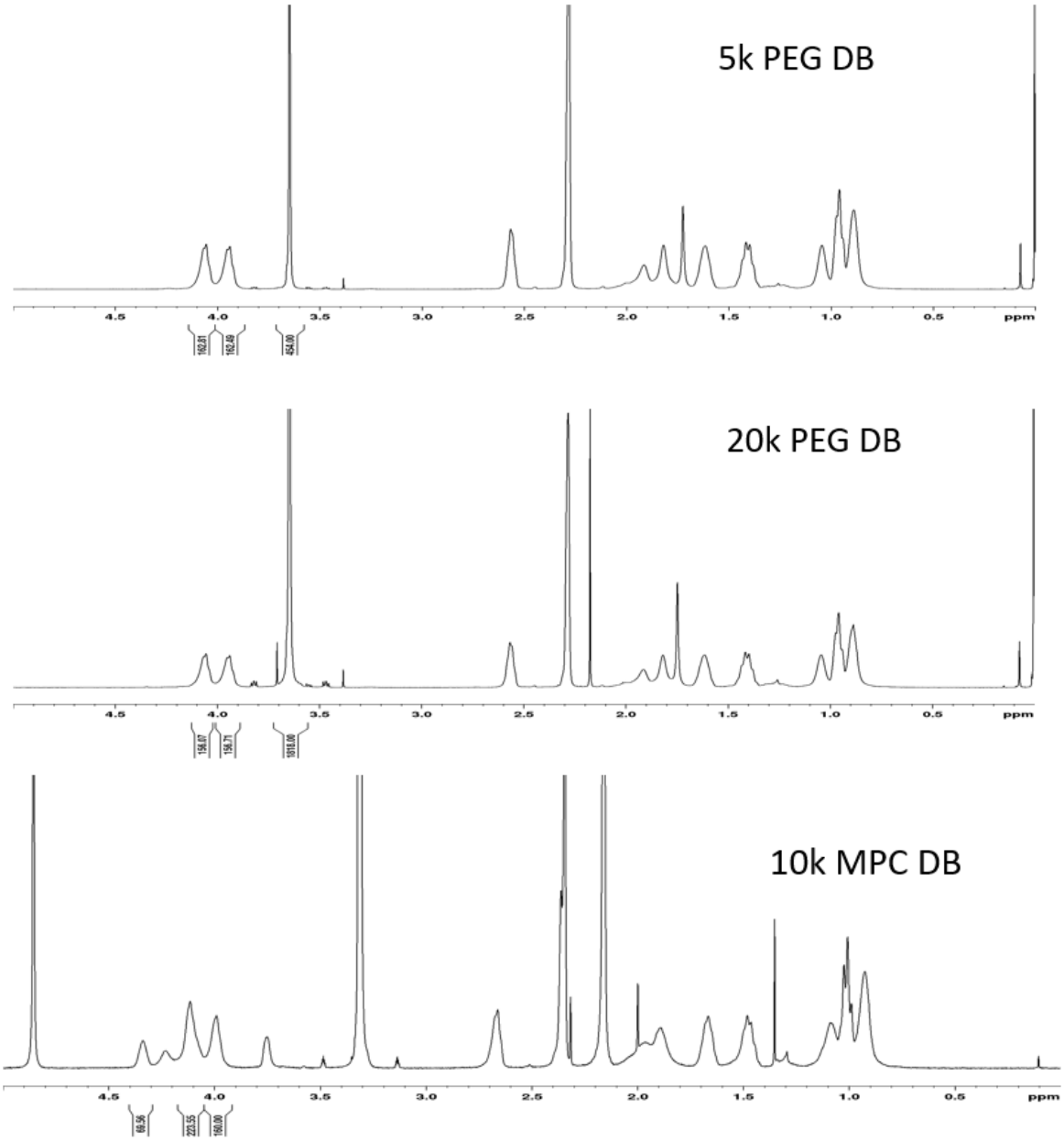

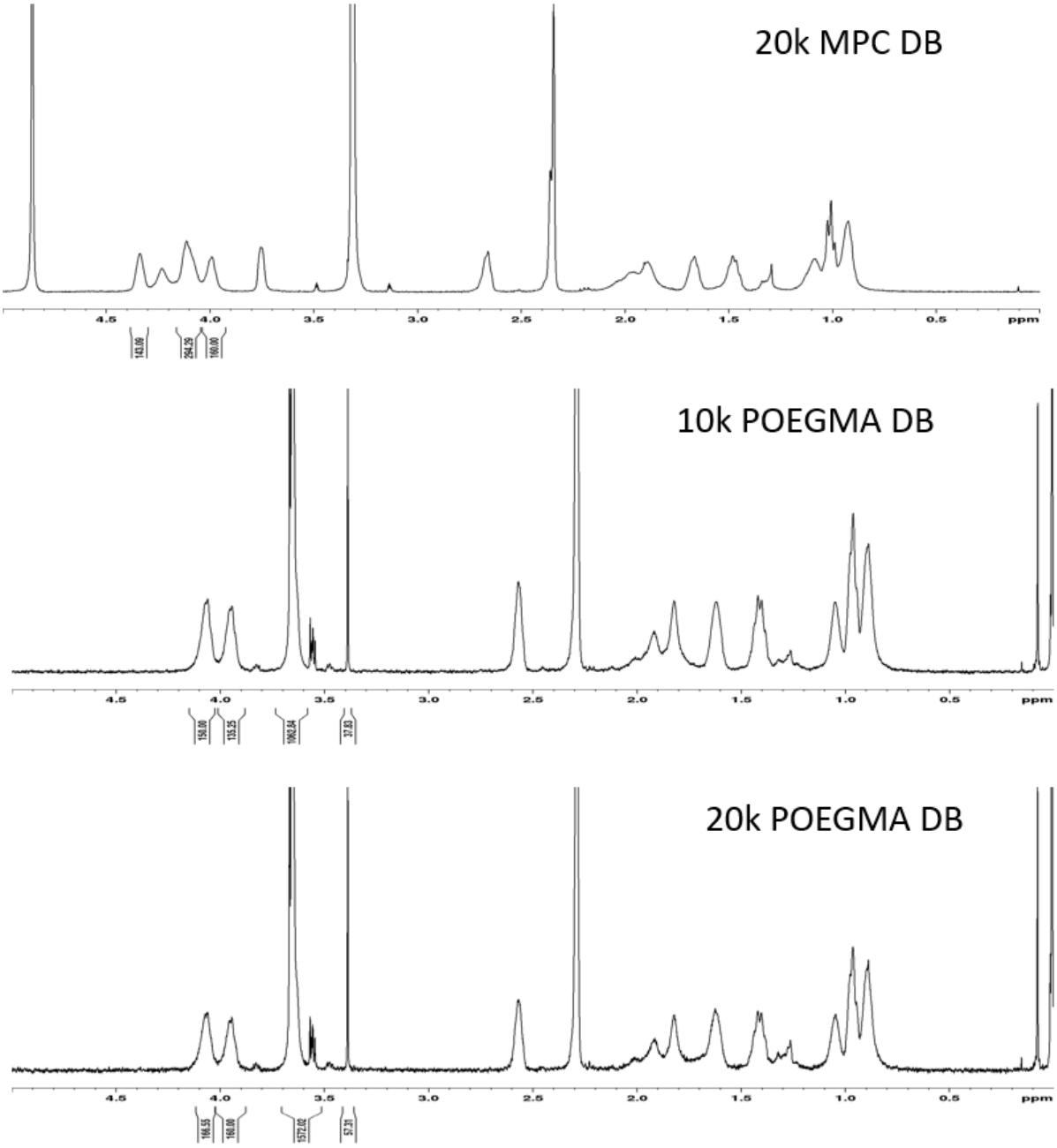
20k MPC DB
4.5
4.0
3.5
3.0
2.5
2.0
1.5
1.0
0.5
ppm
143.06
294.29
160.00
10k POEGMA DB
4.5
4.0
3.5
3.0
2.5
2.0
1.5
1.0
0.5
ppm
159.00
135.25
1062.84
37.83
20k POEGMA DB
4.5
4.0
3.5
3.0
2.5
2.0
1.5
1.0
0.5
ppm
166.55
160.00
1572.02
57.31

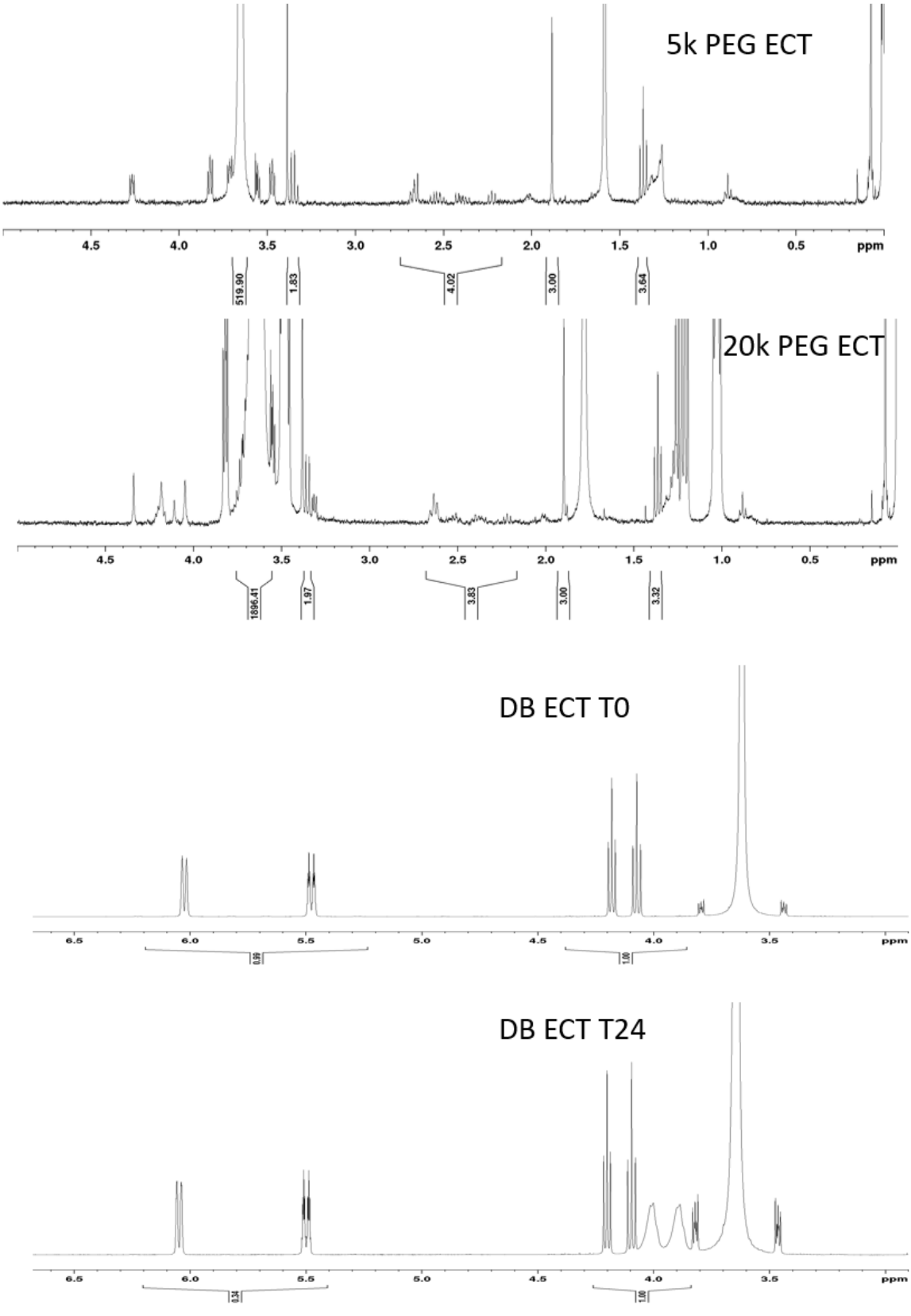
5k PEG ECT
4.5
4.0
3.5
3.0
2.5
2.0
1.5
1.0
0.5
ppm
519.90
1.83
4.02
3.00
3.64
20k PEG ECT
4.5
4.0
3.5
3.0
2.5
2.0
1.5
1.0
0.5
ppm
1886.41
1.97
3.83
3.00
3.32
DB ECT T0
6.5
6.0
5.5
5.0
4.5
4.0
3.5
ppm
0.99
1.00
DB ECT T24
6.5
6.0
5.5
5.0
4.5
4.0
3.5
ppm
0.34
1.00

Supplemental Figure S1: NMR of all polymers synthesized in this work. *Conjugation efficiency for 5k PEG ECT and 20k PEG ECT were 86% and 95 %, respectively. Monomer conversion rate for DB ECT random copolymer was 65%. All NMRs were performed in deuterated chloroform except for 10k MPC DB and 20k MPC DB, which were in MeOD.*

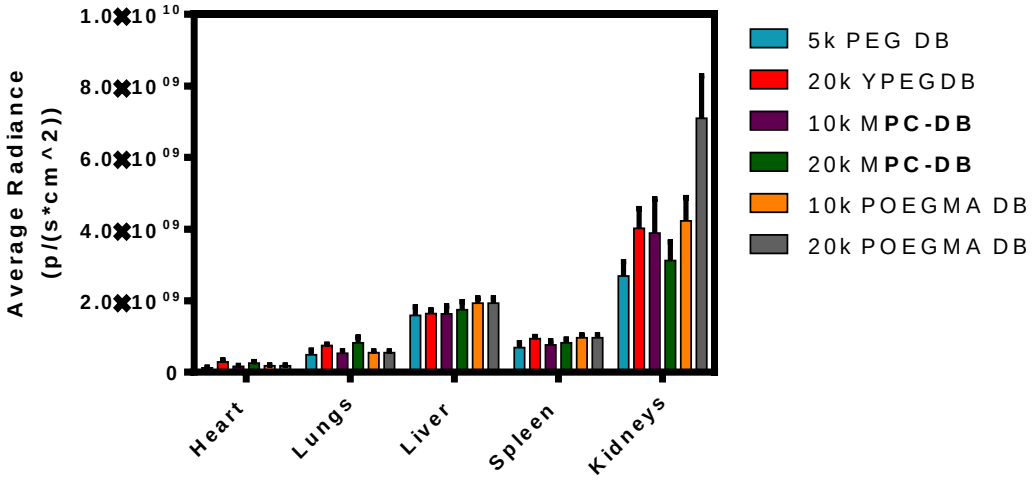

Supplemental Figure S2: Raw average radiance data for polyplexes 20 minutes post-injection. *Overall radiance for 5k PEG DB was already diminished in most organs by 20 minutes compared to other polyplexes.*